nature geoscience | SUPPLEMENTARY INFORMATION
DOI: 10.1038/NGEO2405

Moist convection in hydrogen atmospheres and the frequency of Saturn's giant storms

Cheng Li and Andrew P. Ingersoll

S1. Isobaric mixing across temperature discontinuity at the cloud bottom

In section 2 we discussed convective inhibition due to the mass loading effect: As the troposphere cools, the density just above cloud base first decreases due to the unloading of high-mass molecules by precipitation, creating a stable interface with the fluid just below cloud base. Further cooling reverses this trend, and the stable layer disappears. The question arises, would mixing across the interface hasten the disappearance, thereby destroying the convective inhibition? Because linear mixing between two points on a convex saturation curve produces an over-saturated parcel, the conserved quantities of the mixing process are the total mass and the moist enthalpy[1] defined by:

$$h = C_p T + L_v \eta^*(T)\epsilon \quad \text{(S1.1)}$$

where $\eta^*(T)$ is the saturation water mixing ratio at temperature T . We let f and $1-f$ be the fractions of upper- and lower-layer fluid in the final mixture, respectively. Since f is unknown, we consider the full range from $f=0$ to $f=1$. The temperature of the mixture (T_m) is solved by the equation:

$$f\left[C_p T_1 + L_v \eta^*(T_1)\epsilon\right] + (1-f)\left[C_p T_2 + L_v \eta^*(T_2)\epsilon\right] = C_p T_m + L_v \eta^*(T_m)\epsilon \quad \text{(S1.2)}$$

where T_1 is the temperature above the interface; T_2 is the temperature below the interface; T_m is the temperature of the mixture. As described in section 2, the density variable that determines the stability is the virtual temperature. Let the subscript $(\quad)_v$ stands for virtual temperature. If $T_{mv} > T_{2v}$, the mixture is stable with respect to the air beneath it. If $T_{mv} < T_{1v}$, the mixture is stable with respect to the air above it. Therefore, the mixture is totally stable if:

$$T_{1v} > T_{mv} > T_{2v} \quad \text{(S1.3)}$$

We have considered the mass loading of extra liquid water in the mixture. The temperature T_2 below the interface does not change, but T_1 varies from the warm adiabat (332 K) to the cold adiabat (325 K). We display the value of $T_{mv} - T_{1v}$ and $T_{mv} - T_{2v}$ in Fig. S1.

At the start of the radiative cooling phase, we find that the mixture is always less dense than the fluid below the interface and more dense than the fluid above it, meaning that the interface is stable. However near the end of the cooling phase the mixture is less dense than the fluid above, and the interface is unstable. Depending on the value of f, which is unknown, this could hasten the onset of convection and decrease the time between giant storms by up to 25%. Given the other uncertainties, such as the water vapor mixing ratio at depth, the 25% decrease has no significant effect on the model results.

S2. More details about the numerical model

The axisymmetric primitive equations in log-pressure coordinates are:

$$\frac{\partial u}{\partial t} + u\frac{\partial u}{\partial r} + w\frac{\partial u}{\partial z} - \frac{v^2}{r} - fv = -\frac{\partial \phi}{\partial r} + K_{xx}\nabla^2 \mathrm{u} \tag{S2.1}$$

$$\frac{\partial v}{\partial t} + u\frac{\partial v}{\partial r} + w\frac{\partial v}{\partial z} + \frac{uv}{r} + fu = K_{yy}\nabla^2 v \tag{S2.2}$$

$$\frac{\partial \theta}{\partial t} + u\frac{\partial \theta}{\partial r} + w\frac{\partial \theta}{\partial z} = \theta\frac{\sum_i L_i \epsilon_i \dot{q}_i}{C_p T} \tag{S2.3}$$

$$\frac{\partial \eta_i}{\partial t} + u\frac{\partial \eta_i}{\partial r} + w\frac{\partial \eta_i}{\partial z} = -\dot{q}_i \tag{S2.4}$$

$$\dot{q}_i = \frac{\partial}{\partial t}[\eta_i - min(\eta_i,\ \ \eta_i^*)] \tag{S2.5}$$

$$\frac{\partial \phi}{\partial z} = \frac{RT_v}{H_0} = g\frac{T}{T_0}\frac{1+\sum_i \eta_i}{1+\sum_i \epsilon_i \eta_i} \tag{S2.6}$$

$$T = \theta\left(\frac{p}{p_0}\right)^{\frac{R_d}{C_p}} = \theta \exp\left(-\frac{gz}{C_p T_0}\right) \tag{S2.7}$$

$$\frac{1}{r}\frac{\partial}{\partial r}(ru) + \frac{\partial w}{\partial z} - \frac{z}{H_0} = 0 \tag{S2.8}$$

$$\frac{\partial \psi}{\partial z} = -\rho_0 ru \exp\left(-\frac{z}{H_0}\right), \frac{\partial \psi}{\partial r} = \rho_0 rw \exp\left(-\frac{z}{H_0}\right) \tag{S2.9}$$

where u, v, w are radial, azimuthal and vertical winds. θ, T, T_v are potential temperature, temperature and virtual temperature. ψ is the mass streamfunction; $\rho_0 = 1\ \mathrm{kg/m^3}$. $L_i, \epsilon_i, \eta_i, \eta_i^*, \dot{q}_i$ are microphysical variables. They represent the latent heat, molecular mass ratio to dry air, mole mixing ratio, saturation mixing ratio and condensation rate for condensable species i (i = NH_3, H_2O) respectively. R_d, C_p are the gas constant and specific heat capacity for dry air. $T_0, H_0 = R_d T_0/g$ are the temperature and density scale height at $p_0 = 1$ bar. r, z are the radial distance and log-pressure coordinate: $z = H_0 \ln\frac{p_0}{p}$. ϕ, g are the geopotential height and gravity. Eddy viscosity K_{xx}, K_{yy} are included in the momentum equations to damp out the energy. Since their values are unknown, we choose a small enough value ($K_{xx}/\Delta x^2 = K_{yy}/\Delta y^2 = 3 \times 10^{-3}$) to both maintain numerical stability and damp out the energy. Any value larger than the current one will result in a decrease of the azimuthal wind and the cooling time. Boundary conditions are applied such that pressure gradient vanishes ($\phi = 0$) at the lower boundary and the vertical velocity vanishes ($w = 0$) at the upper boundary due to the strong stratification of the stratosphere[2]. We have moved the lower (upper) boundary low (high) enough to minimize the effects of boundary conditions. Currently, the lower boundary is 30 bars and the upper boundary is 10 mbar. The positions of lower and upper boundary have negligible effects on the result when the lower boundary is placed deeper than 25 bars and the upper boundary higher than 50 mbar. The largest radial distance in the model is 10^7 m and two energy absorbing layers are placed at the top and right part of the domain.

S3. Sensitivity tests for the choices of η and r_0

Fig. S2 has 9 panels showing the equilibrated temperature and azimuthal wind for a 3×3 combination with η being 1.0%, 1.1%, 1.2% and r_0 being 100 km, 200 km, 300 km. Here η is the deep water vapor mixing ratio and r_0 is the Gaussian radius of the initial disturbance. Larger water mixing ratio results in large temperature difference between the warm and cold adiabat, thereby larger wind speed and tropospheric warming. Different values of r_0 do not change the overall structure of the wind and the warming because those variables are largely related to the deformation radius of the atmosphere and are insensitive to the initial conditions such as r_0.

S4. Numerical method of calculating the top cooling scheme

In the section of radiative cooling phase in the manuscript, we presented our scheme for calculating the multi-decadal cooling phase, where the troposphere loses heat from the top. An interface develops between the convecting layers above and the undisturbed layers below. We described the interface moving down through our numerical grid as a two-step process. Step 1 (entrainment step) occurs when the interface is neutrally stable and moves down a level, entraining all the fluid in the grid box below. Step 2 (cooling step) occurs over a period of time and involves lowering the temperature of the fluid above until the interface is neutral again. Here we describe this process in greater detail.

The numerical results calculated by the above scheme at every other grid box are displayed as a time series in Fig. S3. At each time, the left panel (a) shows virtual potential temperature, whose vertical gradient determines whether the column is stable or unstable to convection. The middle panel (b) shows potential temperature, which gives the contribution of temperature alone to the stability of the column. The right panel (c) gives the mixing ratios of water (blue) and ammonia (green). Temperature itself, which falls off monotonically with altitude at all times, is not shown. The primordial profile, following geostrophic adjustment after the last giant storm, is shown as a heavy solid line in the figure for Year = 0.3. This profile becomes a remnant as the interface moves downward and the primordial layer shrinks. The warm and cold moist adiabats—the solid and dashed red lines in Fig. 2 of the main paper—are shown as dotted lines in Fig. S3. There are three characteristic features of the potential temperature profile in panel (b). Above the 1 bar level, the profile is close to the warm adiabat. Between 1 bar and 6 bars, the profile follows a transition from the warm adiabat to the cold adiabat. In pressure levels deeper than 6 bars, potential temperature decreases with depth and contributes to the stability of the column, but then it overshoots and creates a potential temperature minimum at the cloud base. However, this negative potential temperature lapse rate is stable because it is compensated by the increase of the mean molecular weight to deep pressure levels. Therefore, the lapse rate of virtual potential temperature in panel (a) is still positive, and the profile is stable.

The lower boundaries of layers 1, 2, and 3 described in the main text are shown as blue, red, and black triangles, respectively. To visualize the process, it is helpful to click through the entire time series from Year = 0.3 to Year = 74.0. The four layer structure described in the section of radiative cooling phase in the manuscript is best represented at Year = 2.0. Layer 1 is directly subject to radiative cooling at the top. It experience condensation of ammonia and water. Its temperature profile is moist adiabat and the mixing ratio of the constituent is either the saturated value or a constant. Layer 1 is supported by the dry convecting layer 2 below it. Layer 2 has two roles. First, because it is unsaturated, any precipitation in layer 1 will re-evaporate in layer 2. Layer 2 serves as reservoir that holds the extra moisture in layer 1. Column integrated moisture in layers 1 and 2 is conserved. Second, the lower boundary of layer 2 (the interface) separates the convective layers (layers 1 and 2) from the non-convective layers (layer 3) by a jump in temperature and mixing ratios. In the numerical model, the jump is a discontinuity, but in the figure it appears as a steep gradient. Below Layer 2 is layer 3 where the atmosphere is stably stratified and does not convect to mix the minor constituents. Since layer 3 is not disturbed by convection, its temperature and mixing ratio profiles are set by the previous geostrophic adjustment. Layer 3 transits into layer 4 at about 20 bars. Layer 4 is the deep interior, which is a dry adiabat with the minor constituents well mixed. It is somewhat arbitrary to define the precise level of the boundary between layer 3 and layer 4 because the temperature and mixing ratios are continuously changing.

As stated in the main manuscript, the vertical potential temperature profile (shaded region in Fig. S3 after year 9) evolves to lower values than the cold adiabat (left dotted line in Fig. S3a) around year 9, as shown in Fig. S3. However the interface (red triangle) remains stable relative to the cold adiabat. This is because the troposphere is cooling from the top down, with an initial profile that is unsaturated and stable (thick solid line in step #1 of Fig. S3). After year 9, the profile is to the left of the cold adiabat in the upper troposphere, but it crosses to the right in the dry adiabatic layer (between the blue and red triangles), making the interface stable.

Here we present the actual numerical implementation of the above scheme. Suppose the atmospheric column is divided into n discrete cells centered at pressure, $p_i, i = 0 \dots n-1$, from top to bottom. The profile of temperature and mixing ratios are T_i, η_i^a, η_i^w where w represents "water" and a represents "ammonia". These variables are cell averaged quantities from $p_{i-1/2}$ to $p_{i+1/2}$ over the width of the remaining anticyclone after the geostrophic adjustment (section 3). The boundary values between cells are calculated by linear interpolation. We define ϵ^w and ϵ^a as the molecular weights of water and ammonia relative to that of the H_2-He mixture. Then the corresponding mass mixing ratios are:

$$r^a = \frac{\eta^a \epsilon^a}{1 + \eta^a \epsilon^a + \eta^w \epsilon^w}, \qquad r^w = \frac{\eta^w \epsilon^w}{1 + \eta^a \epsilon^a + \eta^w \epsilon^w} \tag{S4.1}$$

Mass per unit area of each cell is:

$$m_i = \frac{p_{i+1/2} - p_{i-1/2}}{g} \tag{S4.2}$$

Column integrated moisture per unit area above the cell k is:

$$Q_k^a = \sum_{i=0}^{k} r_i^a m_i \ , \qquad Q_k^w = \sum_{i=0}^{k} r_i^w m_i \tag{S4.3}$$

Column integrated enthalpy per unit area above the cell k is:

$$H_k = \sum_{i=0}^{k} C_p T_i m_i \tag{S4.4}$$

If the bottom of layer 2 is located at the bottom of cell k: $p = p_{k+1/2}$, then all quantities above that level are determined by $T_k,\ \eta_k^a,\ \eta_k^w$, at pressure p_k. This is because layer 2 is dry adiabatic with constant mixing ratios and layer 1 is moist adiabatic with saturation mixing ratios. One simply follows the dry adiabat up to cloud base—the lifting condensation level for each gas—and then follows the moist adiabat from that point on. This gives $T_i,\ \eta_i^a,\ \eta_i^w, i = 0 \dots k$, so one can calculate $H_k,\ Q_k^a, Q_k^w$.

Let the initial profile of temperature and mixing ratios to be $T_i^0,\ \eta_i^{a,0},\ \eta_i^{w,0}, i = 0 \dots n-1$. We proceed from one entrainment step to the next, during which time the interface moves down from pressure $p_{k-1/2}$ to pressure $p_{k+1/2}$. We assume the preceding entrainment step ended with a stable interface at pressure $p_{k+1/2}$, as indicated by the dashed line in Fig. S3. In other words, the virtual temperature above the interface was greater than that below the interface:

$$T_{k+1/2} \frac{1 + \eta_{k+1/2}^a + \eta_{k+1/2}^w}{1 + \epsilon^a \eta_{k+1/2}^a + \epsilon^w \eta_{k+1/2}^w} \geq T_{k+1/2}^0 \frac{1 + \eta_{k+1/2}^{a,0} + \eta_{k+1/2}^{w,0}}{1 + \epsilon^a \eta_{k+1/2}^{a,0} + \epsilon^w \eta_{k+1/2}^{w,0}} \tag{S4.5}$$

The cycle begins with the slow cooling step, which reduces H_k and T_i, with $\eta_i^a,\ \eta_i^w, i = 0 \dots k$ adjusted to maintain the dry/moist adiabat and conserved the total moisture per unit area:

$$Q_k^a = Q_k^{a,0}, \qquad Q_k^w = Q_k^{w,0} \tag{S4.6}$$

where $Q_k^{a,0},\ Q_k^{w,0}$ are the initial column-integrated moisture per unit area. When equation (S4.5) becomes an equality, as indicated by the thin solid line in Fig. S3, the cooling step ends and the next entrainment step begins. The proper temperature and moistures at cell k: $T_k,\ \eta_k^a,\ \eta_k^w$, when the cooling step ends, are solved using Newton's iteration method to satisfy equations (S4.5) and (S4.6). After we solved for these quantities, we can go for the vertical profiles of $T_i,\ \eta_i^a,\ \eta_i^w, i = 0 \dots k$ by following a dry adiabat and then moist adiabat. The column-integrated enthalpy per unit area is bookkept as H_k^+ using equation (S4.4).

The entrainment process moves the interface down to pressure $p_{k+3/2}$. The new column-integrated enthalpy and column-integrated moisture per unit area are

$$H_{k+1} = H_k^+ + C_p T_{k+1}^0 m_{k+1} \tag{S4.7}$$

$$Q_{k+1}^a = Q_k^{a,0} + r_{k+1}^{a,0} m_{k+1}, \qquad Q_{k+1}^w = Q_k^{w,0} + r_{k+1}^{w,0} m_{k+1} \tag{S4.8}$$

where $r_{k+1}^{a,0}$, $r_{k+1}^{w,0}$ are the initial mass ratios. One then solves, iteratively, for the new values of T_{k+1}, η_{k+1}^a, η_{k+1}^w that give the values on the left sides equations (S4.7) and (S4.8). The interface is now at pressure $p_{k+3/2}$. The elapsed time $\Delta\tau_k$ during this cycle is computed from the decrease in H_k needed to drive the inequality in equation (S4.5) to equality, i.e.:

$$\Delta\tau_k = \frac{\Delta H_k}{Flux} = \frac{H_k - H_k^+}{Flux}, \qquad Flux = 4.5\ \mathrm{W/m^2} \tag{S4.9}$$

If the virtual temperature above this new interface is smaller than the virtual temperature below it, the interface is unstable. Then the interface moves one cell further down and the entrainment step repeats until a stable interface is found or the interface reaches the deep interior.

S5. Discussion about the 6 occurrence of giant storms in the northern hemisphere

We feel that the occurrence in the northern summer could be a statistical fluke complicated by the difficulty of using discrete statistics on hard-to-define phenomena in a turbulent fluid. Sanchez-Lavega[3] defines a Great White Spot as "a kind of rarely-observed disturbance that rapidly grows and expands zonally from a single outburst site, and whose visual appearance is that of a complex pattern of bright white clouds confined to a large latitude band that breaks with the usual banded telescopic aspect of the planet." From 2004 to 2010, Cassini observed lightning storms near the center of the westward jet at 35$^{\mathrm{o}}$ in the southern hemisphere, but not at any other latitude. The season was southern summer in 2004 and early autumn in 2010, so not all activity is in the northern hemisphere. The 1876 storm had the shortest lifetime of 26 days, and until the 2010-2011 storm, the 1903 storm had the longest lifetime of 150 days. The lifetime of the 2010-2011 storm was ~200 days. The fact that we are dealing with real phenomena in a turbulent fluid adds uncertainty to statistical inferences. Even if we were dealing with six coin flips, the probability of their all coming out the same is 1/32. Since one of the great storms was at a latitude of 2 ± 3°N, the number of coins should probably be reduced to five, for which the probability of their all falling in one hemisphere is 1/16. What seems more likely to us is a preference for the sunlit hemisphere, with a statistical fluke favoring the north. A preference for the sunlit hemisphere and for the extrema of the zonal jets might have a physical basis, but we leave that for another paper.

S6. Discussion about radiative heat transfer near the cloud base

Guillot[4] points out that the giant planets might not be fully convective—that at some levels the radiative opacity is small enough that the internal heat flux could be carried by radiation. For Saturn, they show that a radiative zone could develop in the layer from 300 K < T < 450 K, which spans cloud base according to our Fig. 2. Then the cooling shown in Figs. 5 and S3 might not occur, and the atmosphere above cloud base might reach a steady state, with 4.5 W m^{-2} coming in at the bottom and 4.5 W m^{-2} going out at the top. The interface at cloud base, stabilized by the molecular weight gradient, would never cool enough to initiate a giant storm. In this situation, one should remember that atmospheric temperature profile has CAPE, which means it has the potential to convect when the stable interface is broken by other mechanism such as the re-evaporation of condensates from above[5].

However, the existence of a radiative zone is uncertain. It vanishes if water clouds are present around this level, as shown in Fig. 6 of Guillot. If it vanishes, then giant storms can occur. If radiation delivers more than zero but less than the 4.5 W m^{-2} needed to maintain steady state, then the layers above will still cool but at a slower rate. This lengthens the interval between giant storms, but it does not prevent them.

Despite the uncertainty, we shall assume that the time between giant storms is set by the time it takes the atmosphere to cool from the warm adiabat to the cold one, as illustrated in Fig. 2.

Reference

1 Emanuel, K. A. *Atmospheric convection*. (Oxford University Press, 1994).

2 Achterberg, R. K. & Ingersoll, A. P. A Normal-Mode Approach to Jovian Atmospheric Dynamics. *J Atmos Sci* **46**, 2448-2462 (1989).

3 Sanchez-Lavega, A. Saturn's Great White Spots. *Chaos* **4**, 341-353 (1994).

4 Guillot, T., Gautier, D., Chabrier, G. & Mosser, B. Are the Giant Planets Fully Convective. *Icar* **112**, 337-353 (1994).

5 Sugiyama, K., Nakajima, K., Odaka, M., Kuramoto, K. & Hayashi, Y. Y. Numerical simulations of Jupiter's moist convection layer: Structure and dynamics in statistically steady states (vol 229, pg 71, 2014). *Icar* **231**, 407-408 (2014).

Table S1:

Resolution	Azimuthal wind (m/s)	Min T (K)	Max T (K)
64x64	56.8	-6.6	7.3
128x128	81.1	-6.5	8.1
256x128	83.6	-8.1	8.4

Figure legends

Figure S1: Mixing diagram across the temperature discontinuity at the cloud base. X-axis is the temperature above the cloud base (T_1) and y-axis is the fraction of the parcel coming from the top (f). The lower and upper limit of the temperature axis is chosen to be the temperature of the cold and the warm adiabat at the cloud base. The solid curves show $T_{mv} - T_{2v}$, which is always positive. The colored contours show $T_{mv} - T_{1v}$, which is positive (red) to the left and negative (blue) to the right. The mixture is stable (unstable) with respect to the atmosphere above cloud base in the blue (red) zones, respectively.

Figure S2: Residual azimuthal wind (dashed contours) and temperature anomaly (colored contours) for different combinations of parameters. The parameters are indicated at the bottom of each panel.

Figure S3: A series of cooling steps. Panel (a) and Panel (c) represent the same quantity in Fig. 5. Panel (b) is the potential temperature defines as $\theta = T\left(\frac{p_0}{p}\right)^{R/C_p}$. $p_0 = 1$ bar, is the reference temperature. Two dotted lines represent the cold and warm moist adiabat as those in Fig. 2. The thick solid red line is the potential temperature profile after the geostrophic adjustment. The shaded region shows one cooling step, from right to left. The right boundary (dashed line) shows the profile after the preceding entrainment step. The left boundary (solid line) shows the profile just before the next entrainment step. Only stable interfaces are shown in this figure.

Table legend

Table 1: Resolution dependency test. Tabulated values are maximum azimuthal wind, minimum temperature anomaly and maximum temperature anomaly for 3 different resolutions. The first number in the resolution is the horizontal points and the second number is the vertical points.

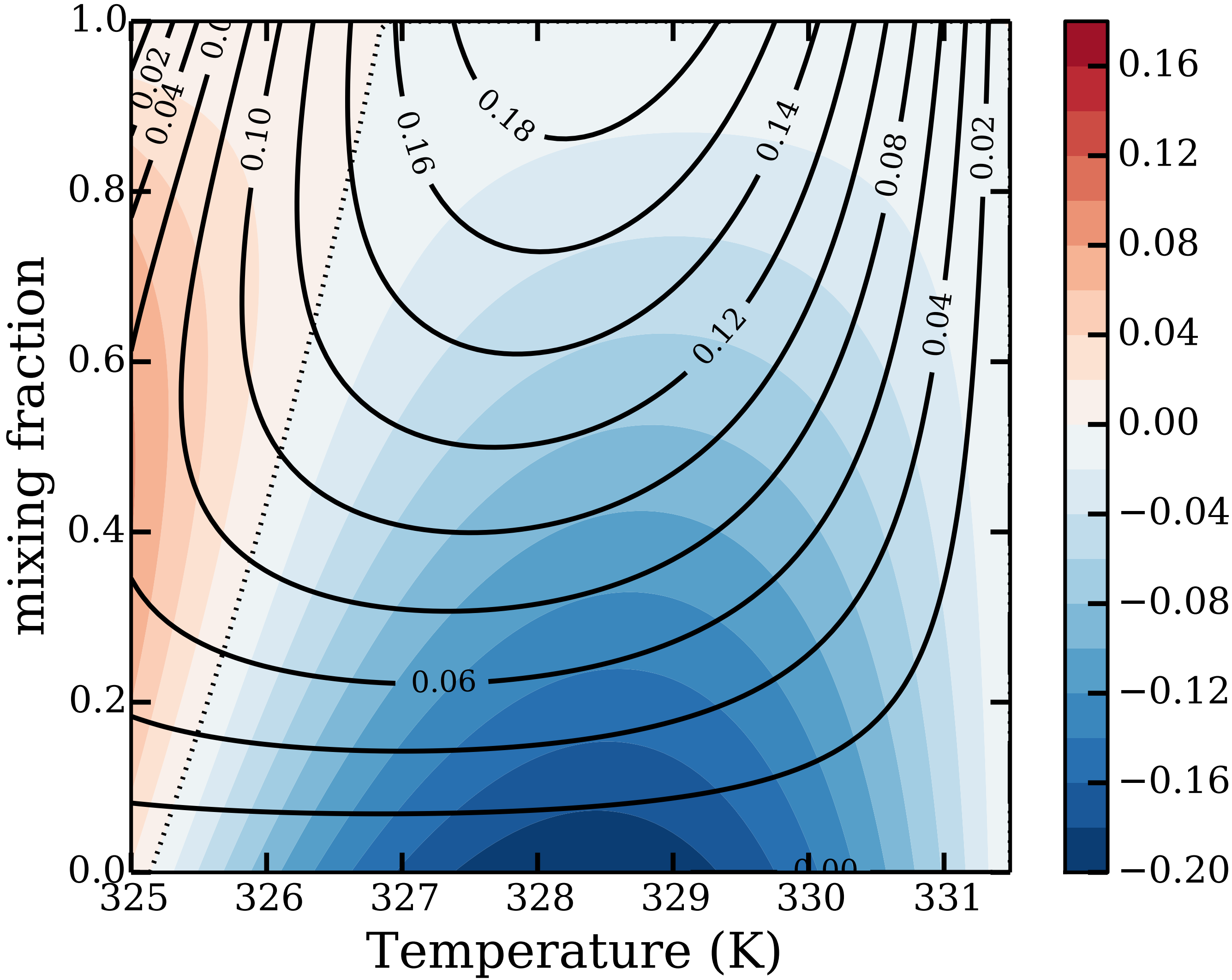

mixing fraction
Temperature (K)
0.02
0.04
0.10
0.16
0.18
0.14
0.08
0.02
0.12
0.04
0.06
0.00

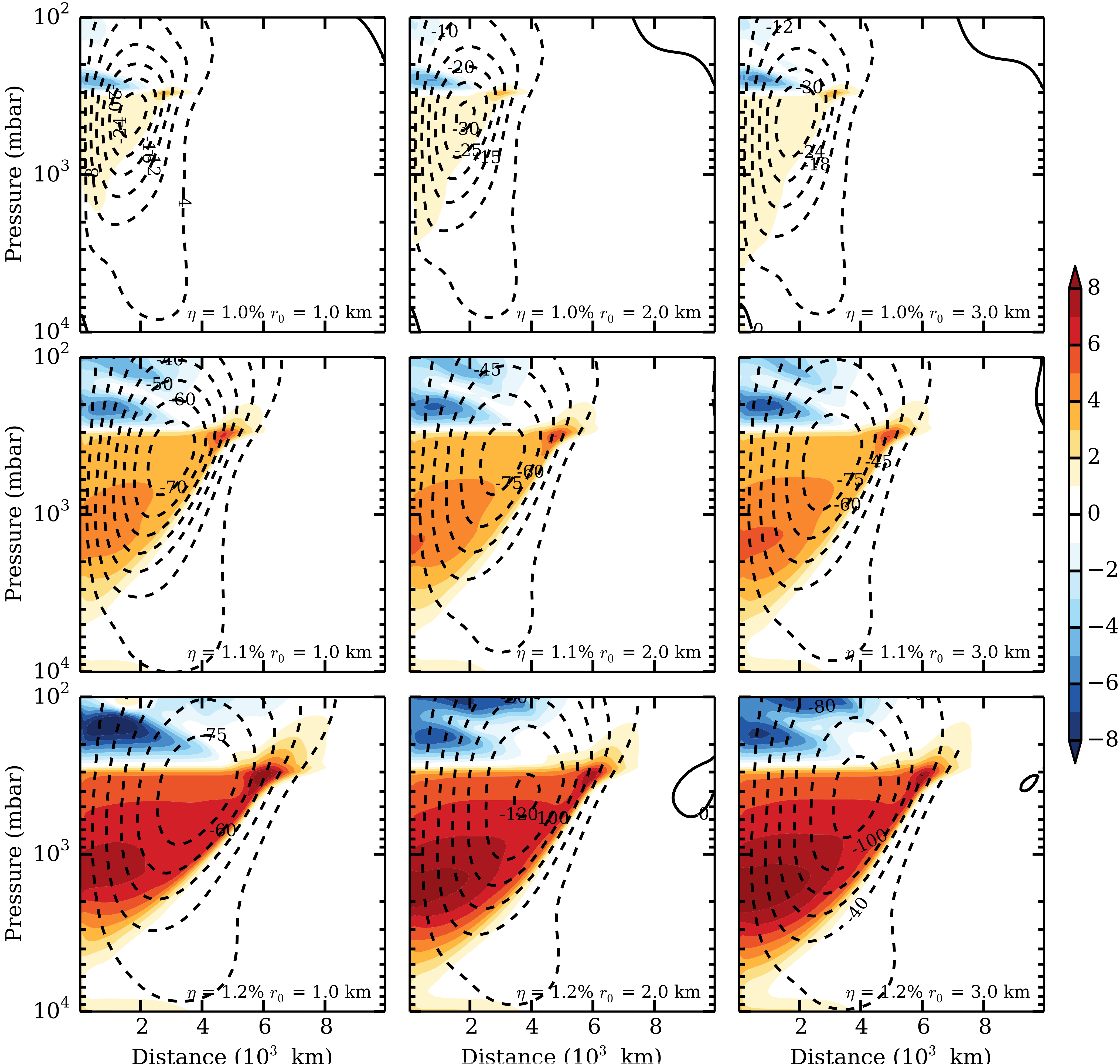

Pressure (mbar)
Distance (10^3 km)
η = 1.0% r_0 = 1.0 km
η = 1.0% r_0 = 2.0 km
η = 1.0% r_0 = 3.0 km
η = 1.1% r_0 = 1.0 km
η = 1.1% r_0 = 2.0 km
η = 1.1% r_0 = 3.0 km
η = 1.2% r_0 = 1.0 km
η = 1.2% r_0 = 2.0 km
η = 1.2% r_0 = 3.0 km

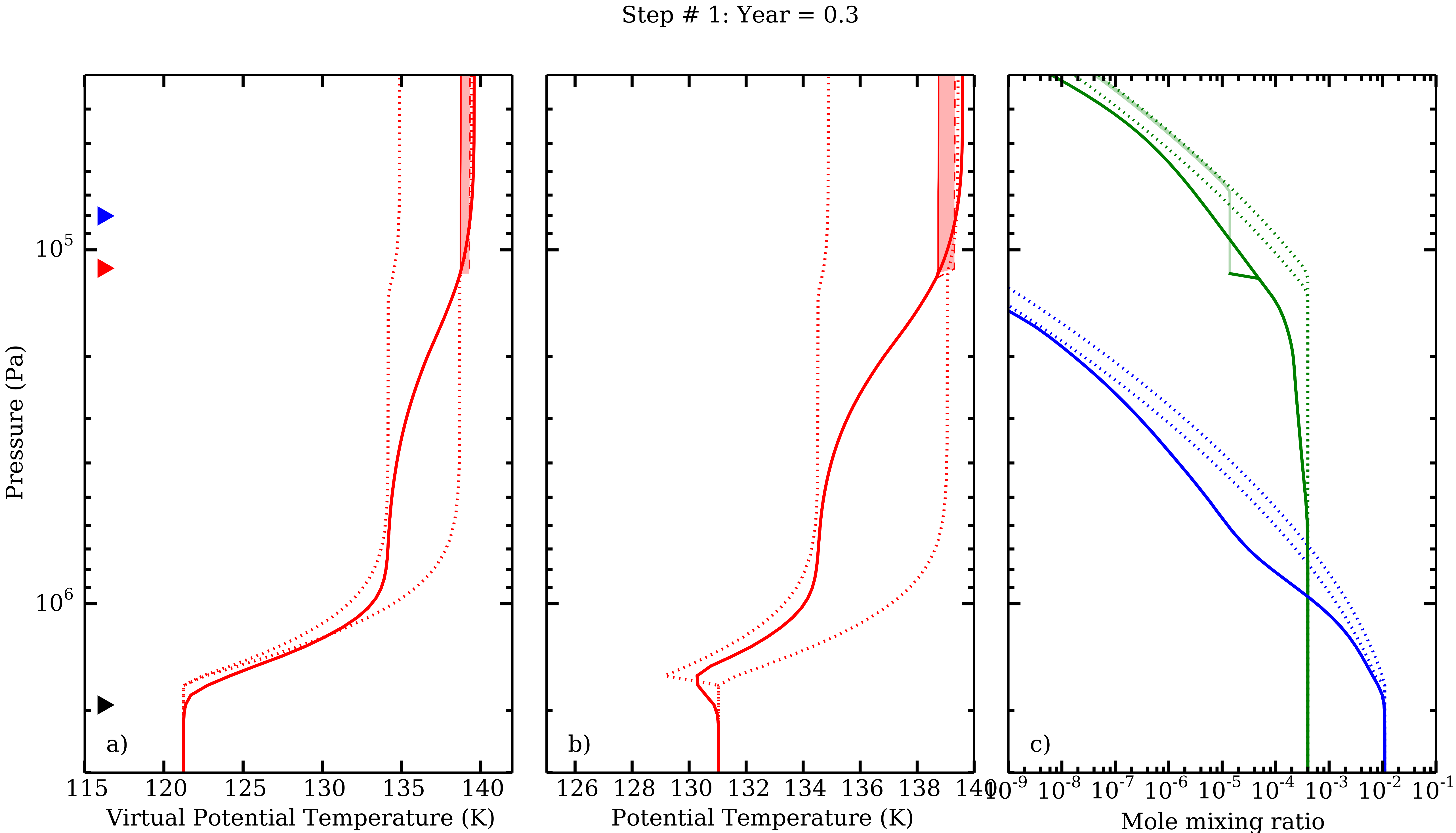

Step # 1: Year = 0.3
Pressure (Pa)
10^5
10^6
a)
115 120 125 130 135 140
Virtual Potential Temperature (K)
b)
126 128 130 132 134 136 138 140
Potential Temperature (K)
c)
10^{-9} 10^{-8} 10^{-7} 10^{-6} 10^{-5} 10^{-4} 10^{-3} 10^{-2} 10^{-1}
Mole mixing ratio

Step # 2: Year = 0.6

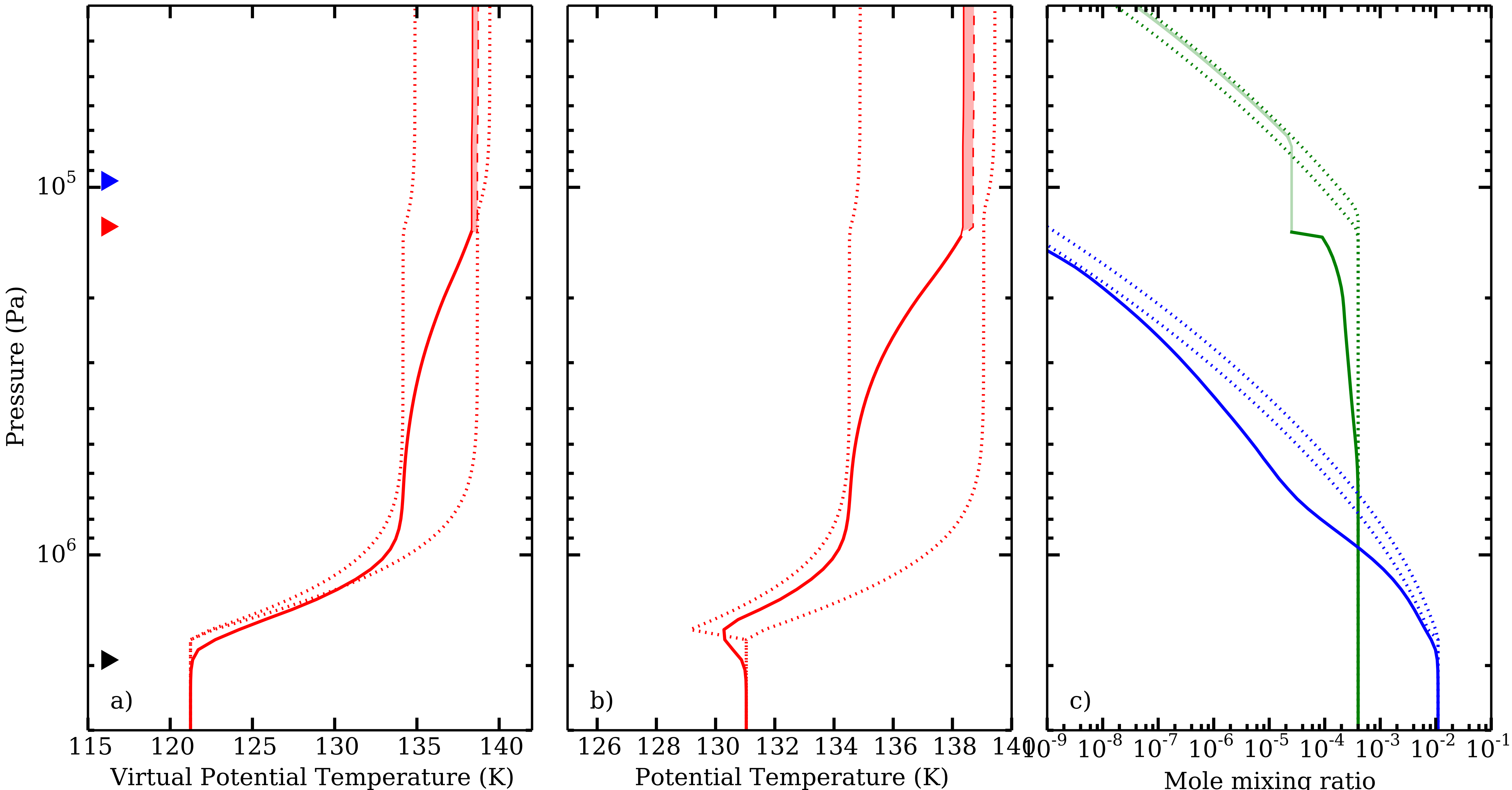

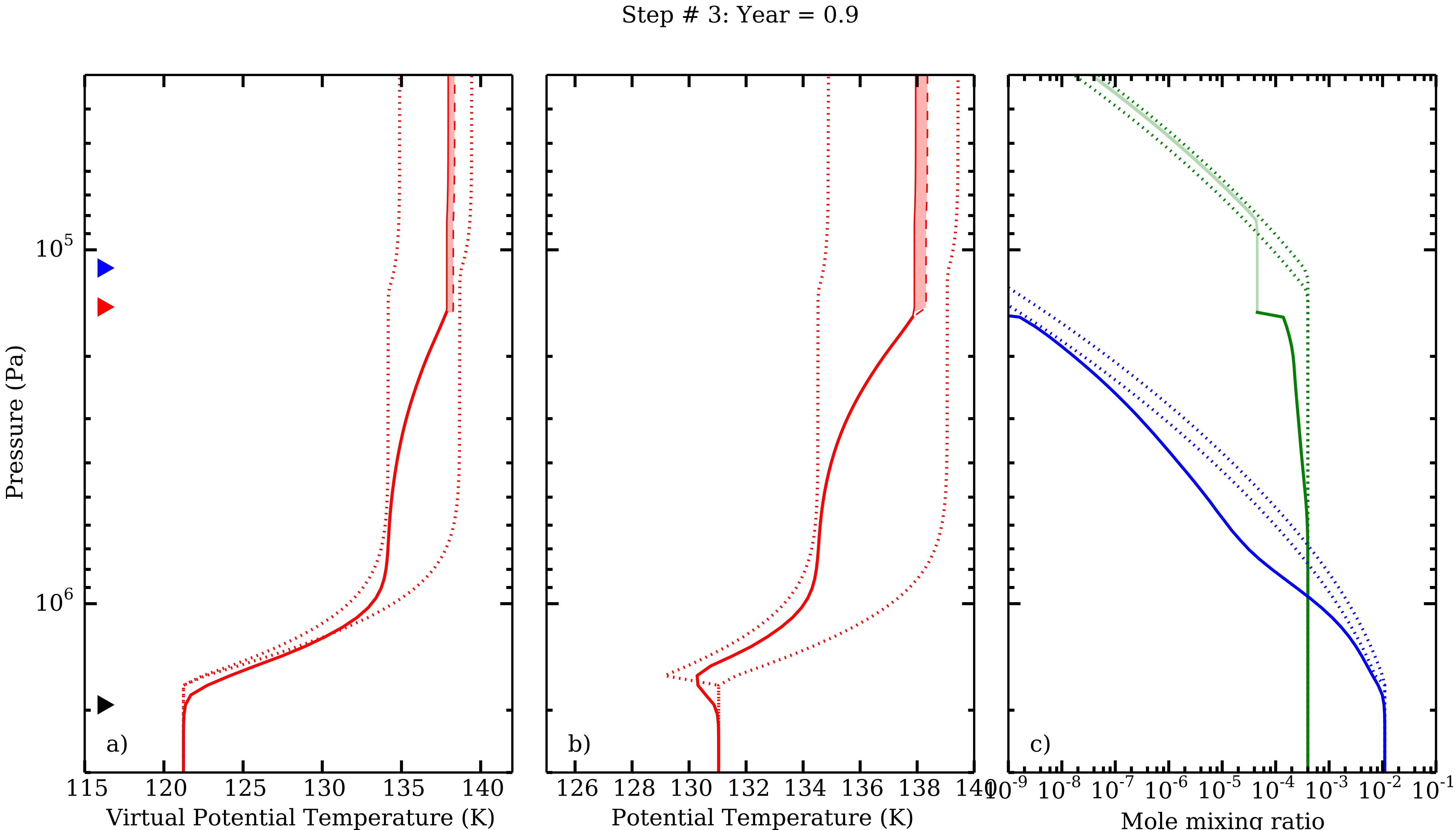

Step # 3: Year = 0.9
Pressure (Pa)
10^5
10^6
a)
115 120 125 130 135 140
Virtual Potential Temperature (K)
b)
126 128 130 132 134 136 138 140
Potential Temperature (K)
c)
10^{-9} 10^{-8} 10^{-7} 10^{-6} 10^{-5} 10^{-4} 10^{-3} 10^{-2} 10^{-1}
Mole mixing ratio

Step # 4: Year = 1.4

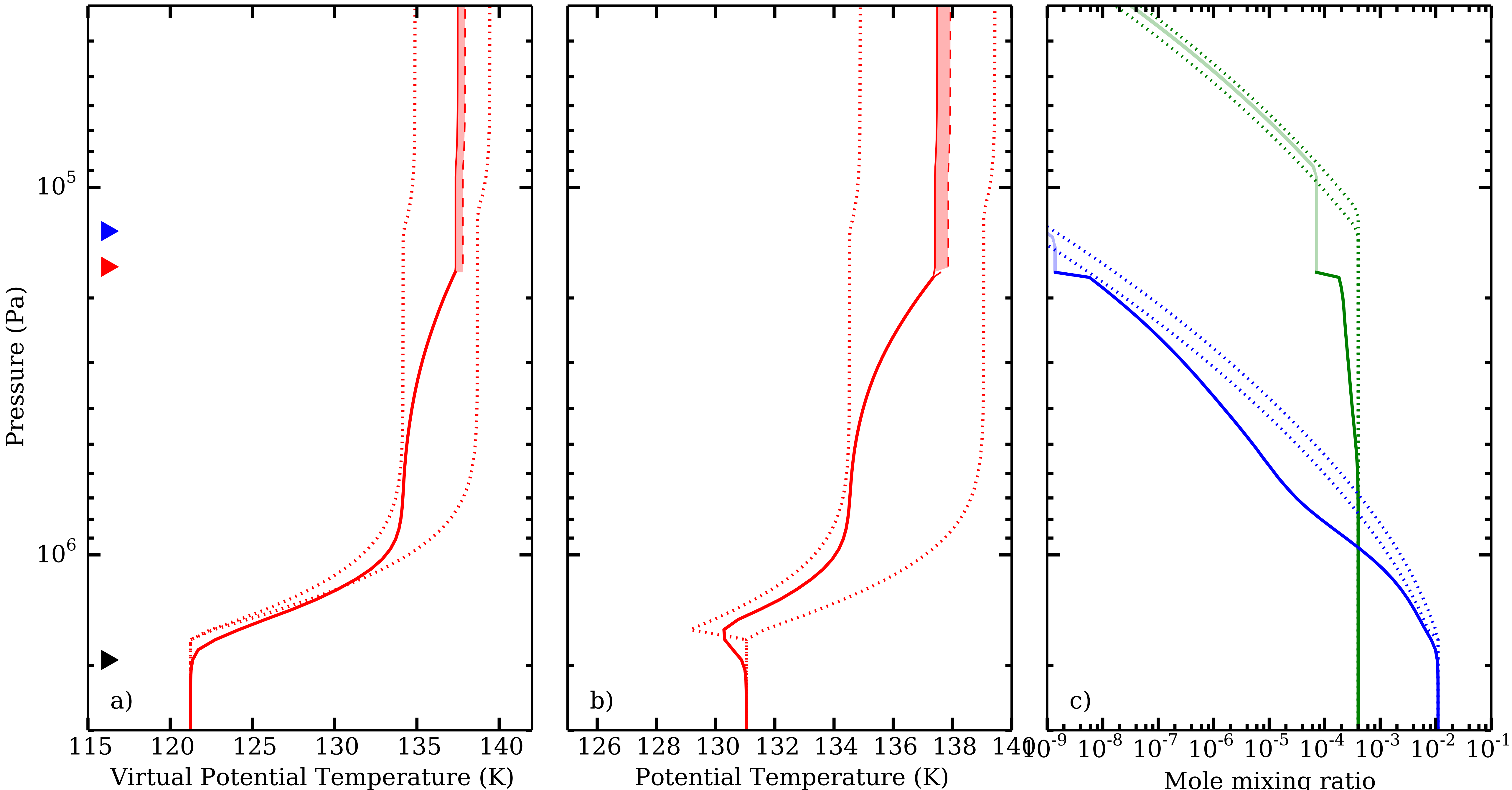

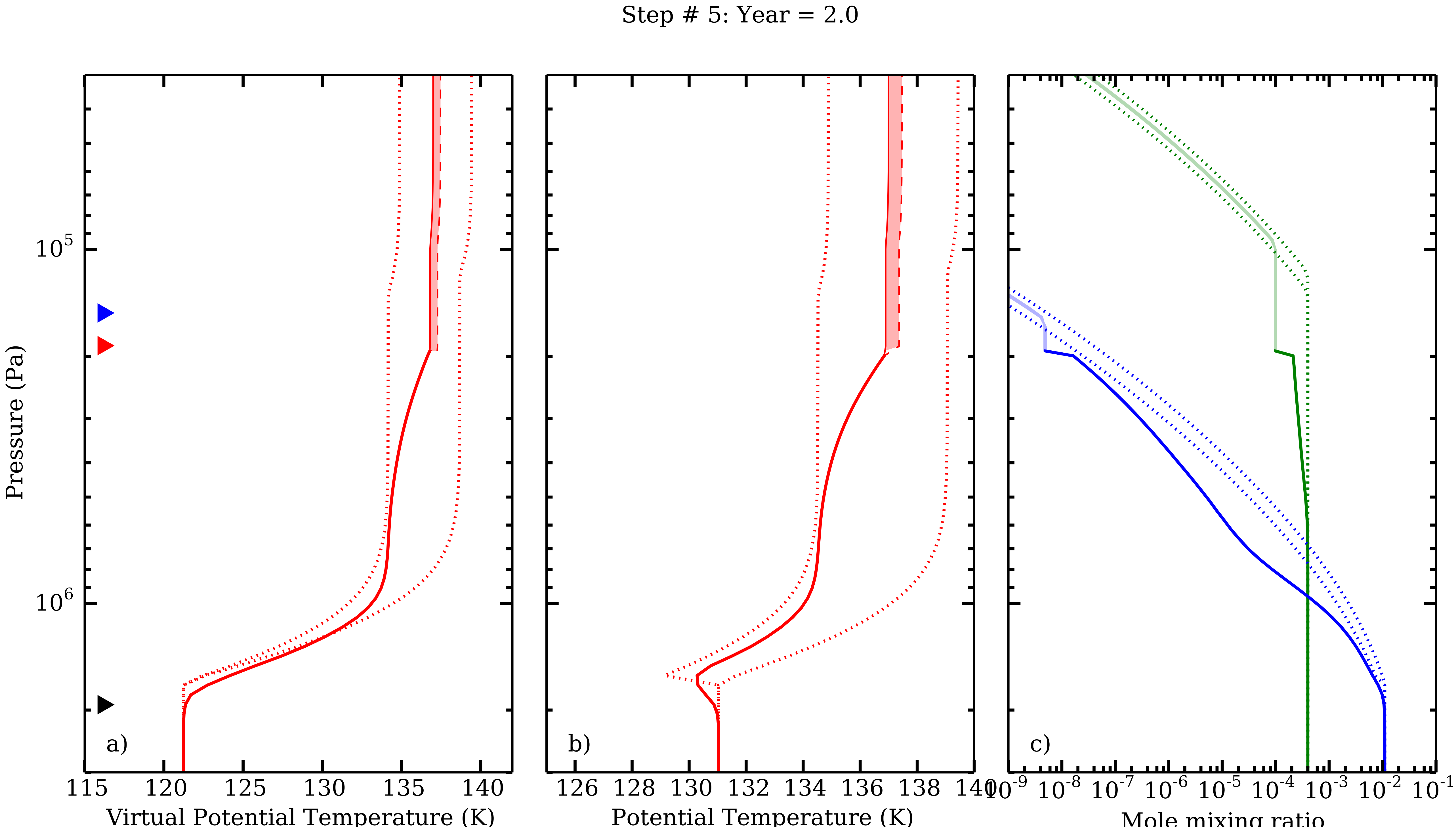

Step # 5: Year = 2.0
Pressure (Pa)
10^5
10^6
a)
115 120 125 130 135 140
Virtual Potential Temperature (K)
b)
126 128 130 132 134 136 138 140
Potential Temperature (K)
c)
10^{-9} 10^{-8} 10^{-7} 10^{-6} 10^{-5} 10^{-4} 10^{-3} 10^{-2} 10^{-1}
Mole mixing ratio

Step # 6: Year = 2.7

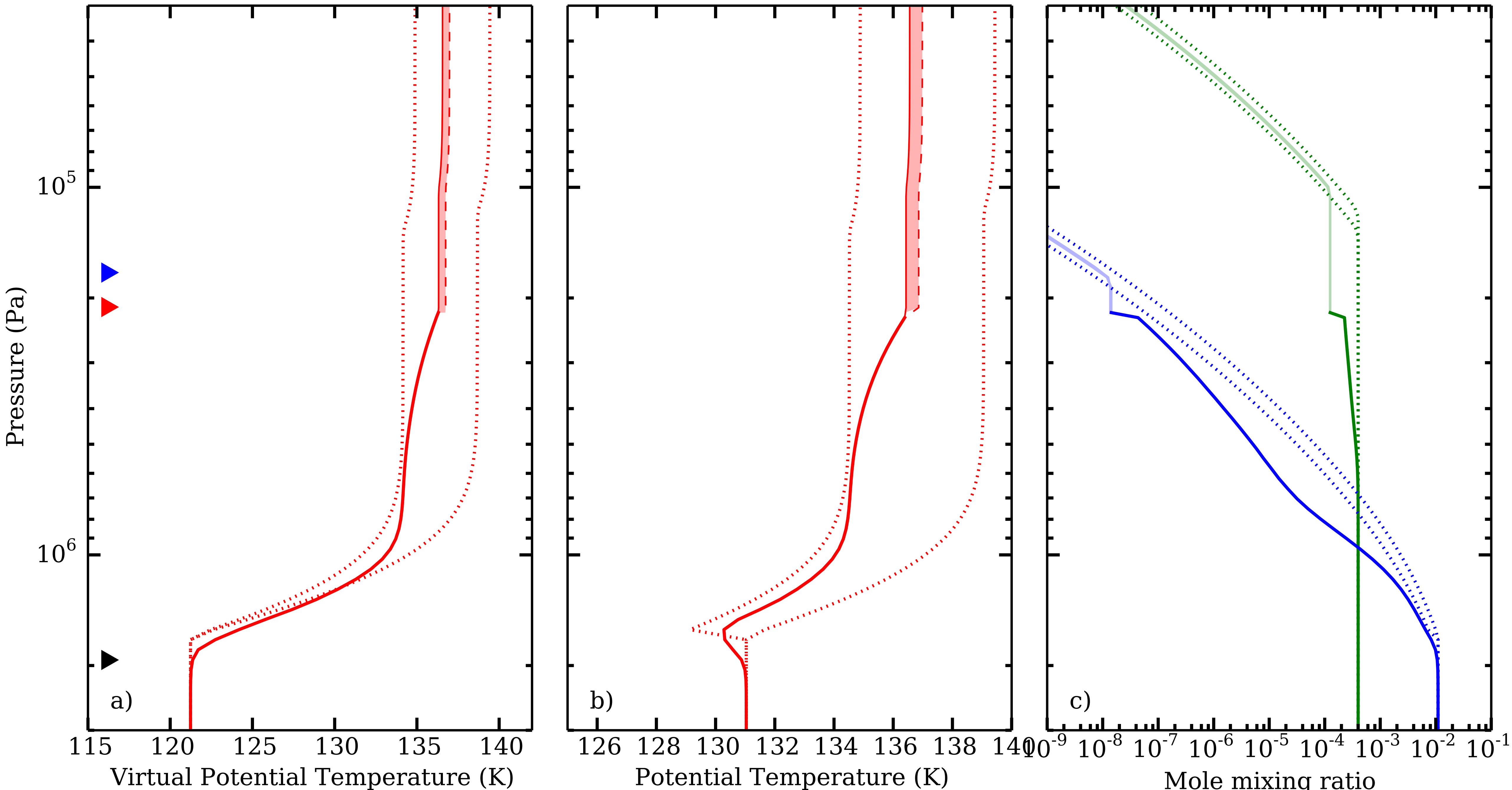

Step # 7: Year = 3.4

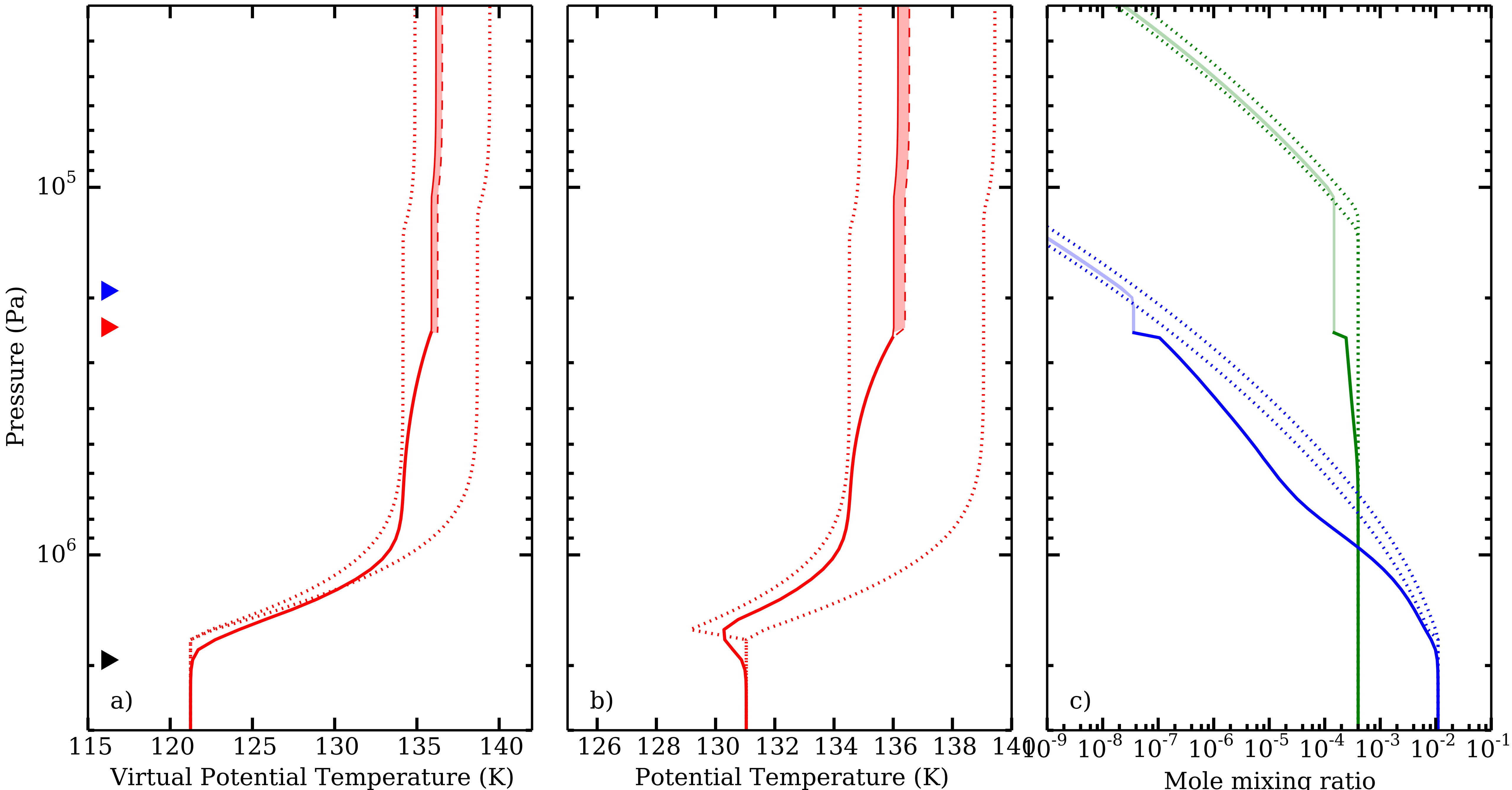

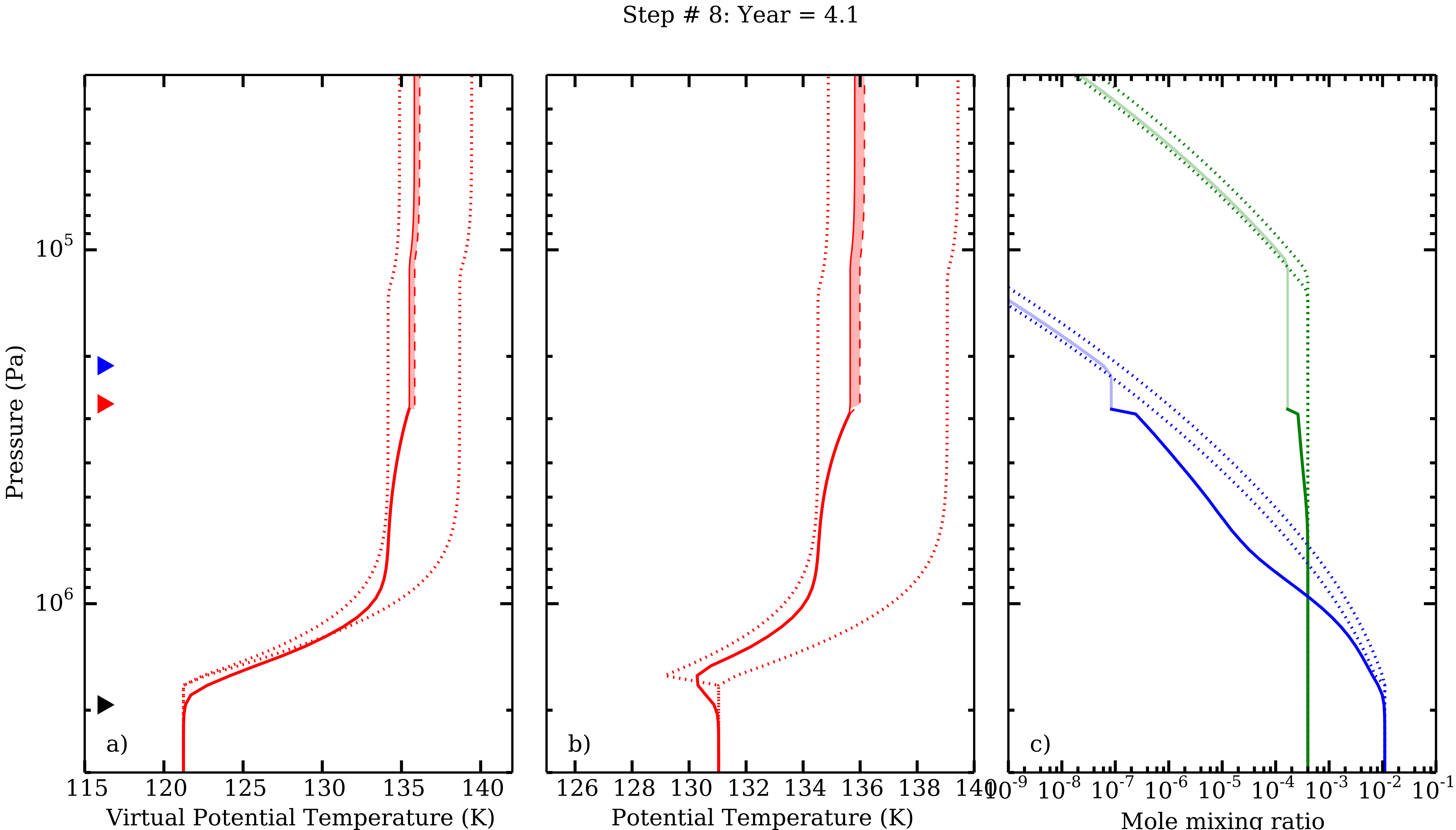
Step # 8: Year = 4.1
Pressure (Pa)
10^5
10^6
a)
115 120 125 130 135 140
Virtual Potential Temperature (K)
b)
126 128 130 132 134 136 138 140
Potential Temperature (K)
c)
10^{-9} 10^{-8} 10^{-7} 10^{-6} 10^{-5} 10^{-4} 10^{-3} 10^{-2} 10^{-1}
Mole mixing ratio

Step # 9: Year = 4.9

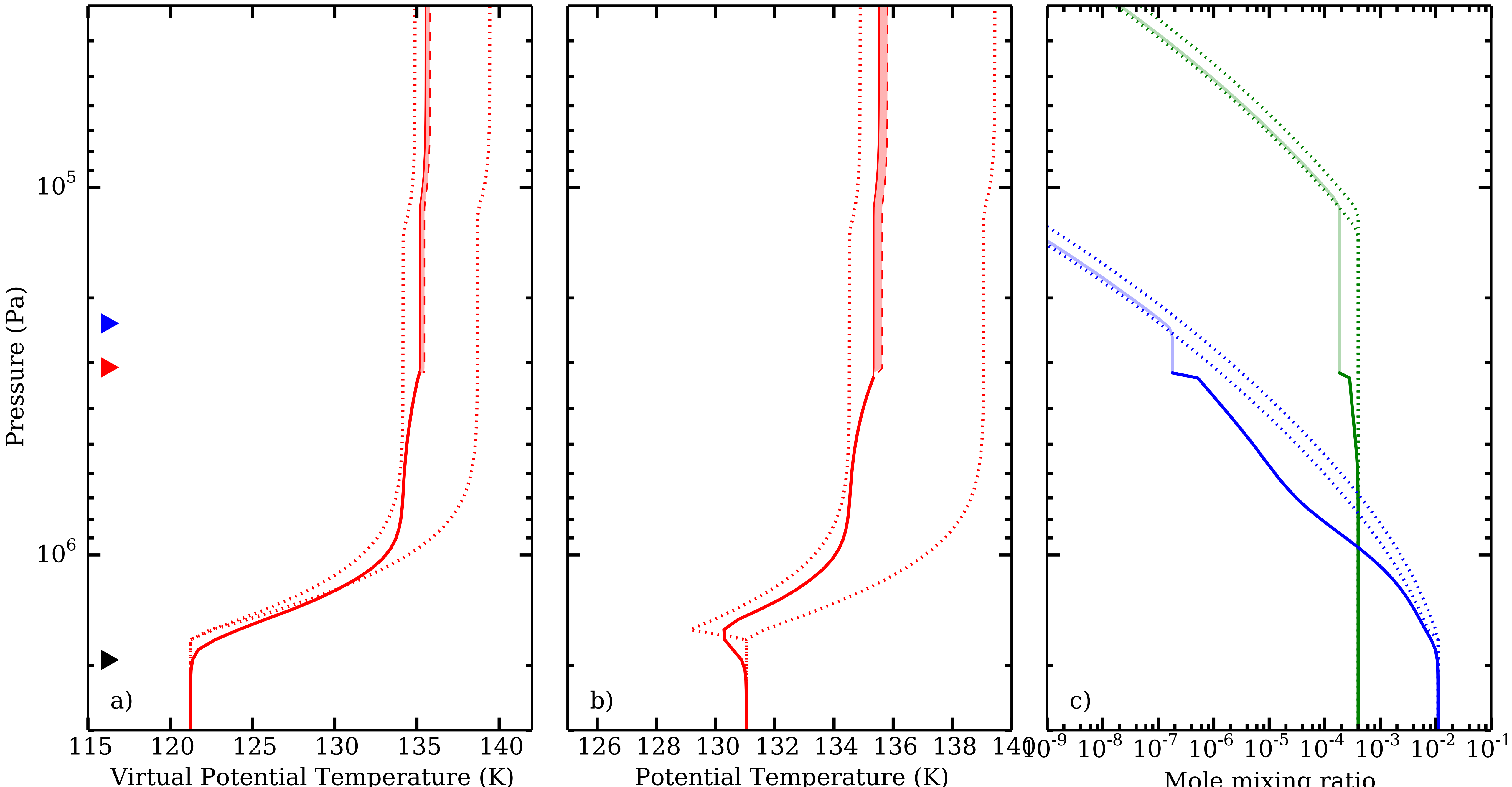

Step # 10: Year = 5.6

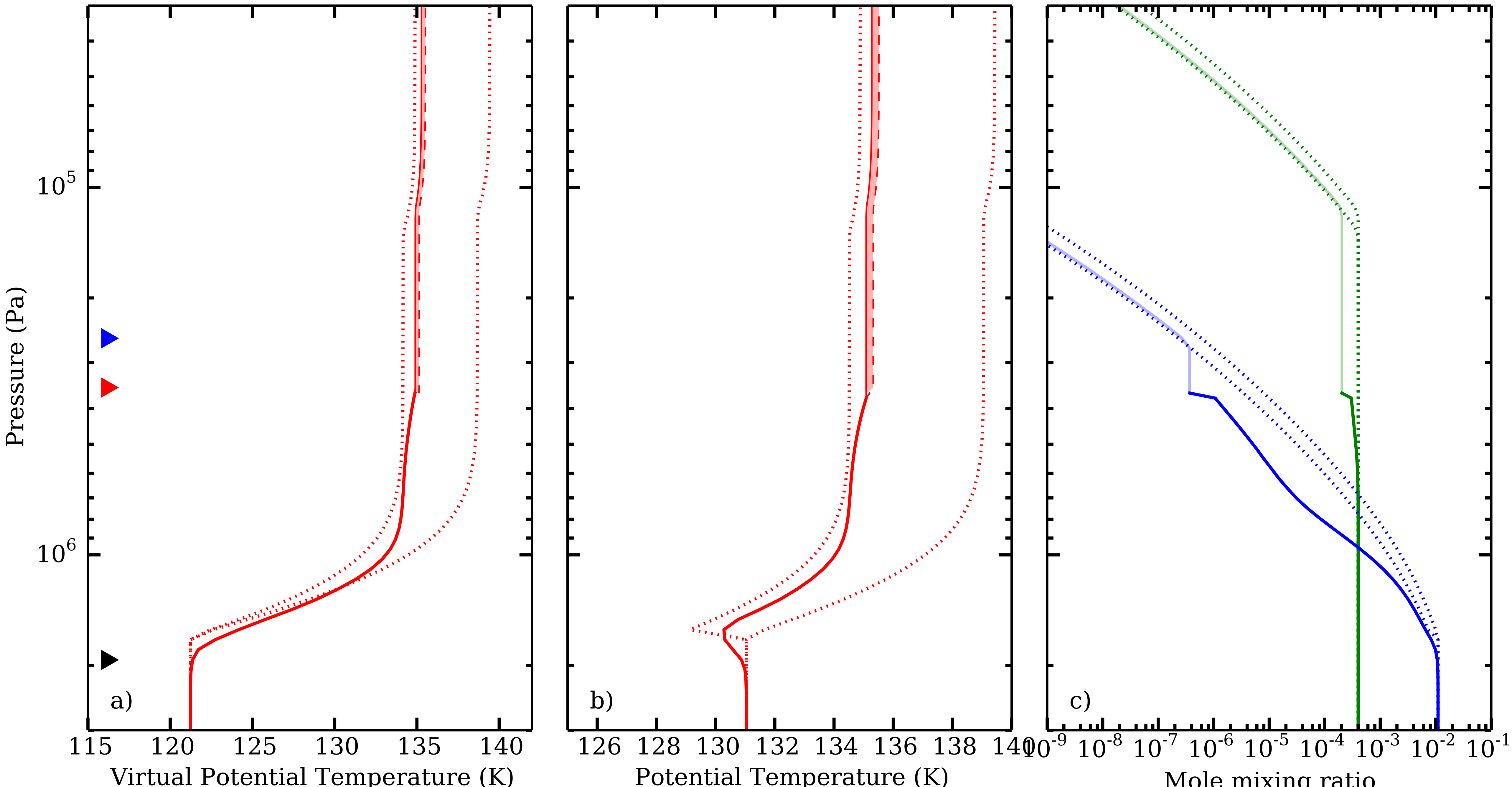

Step # 11: Year = 6.3

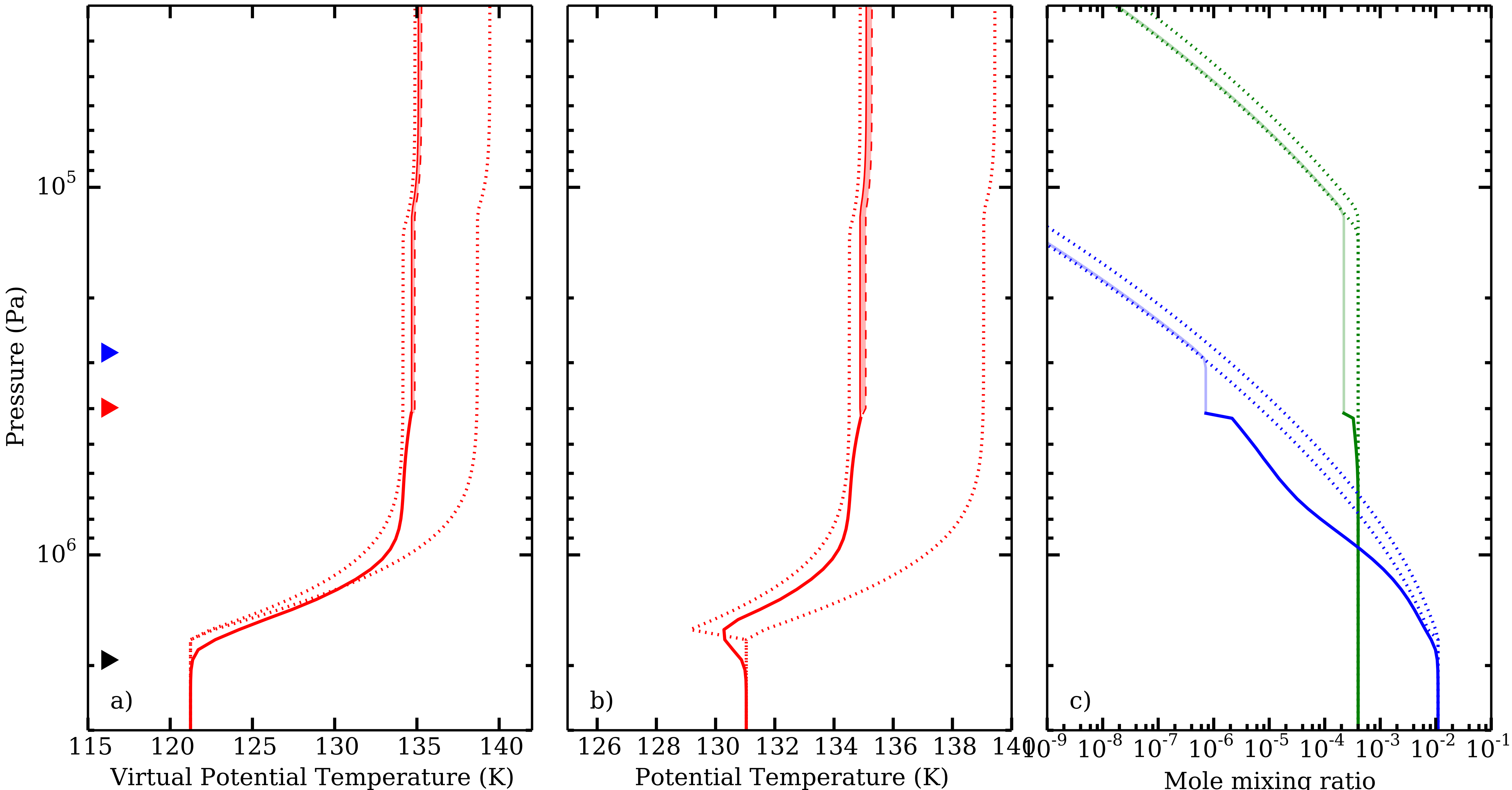

Step # 12: Year = 7.0

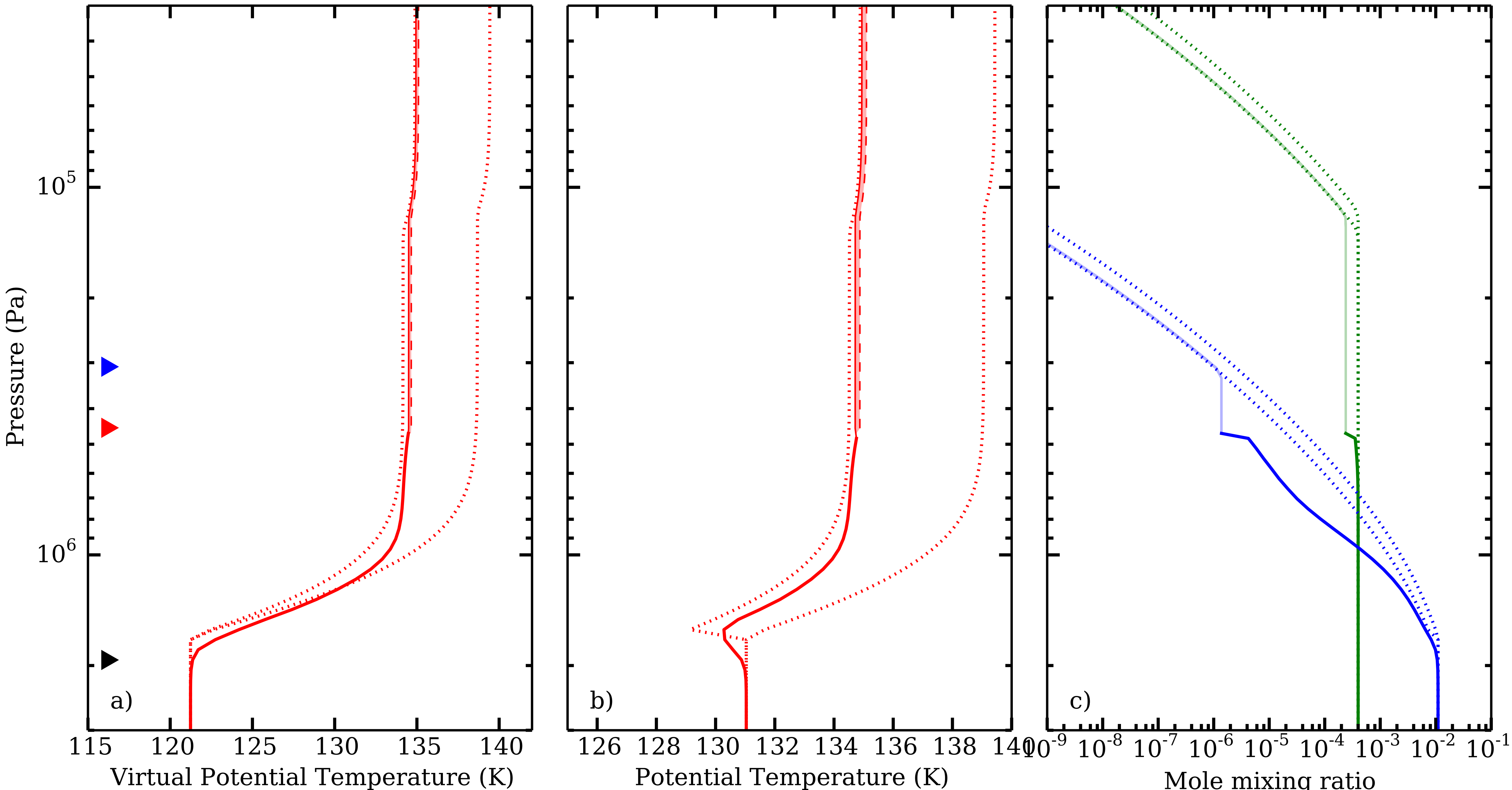

Step # 13: Year = 7.7

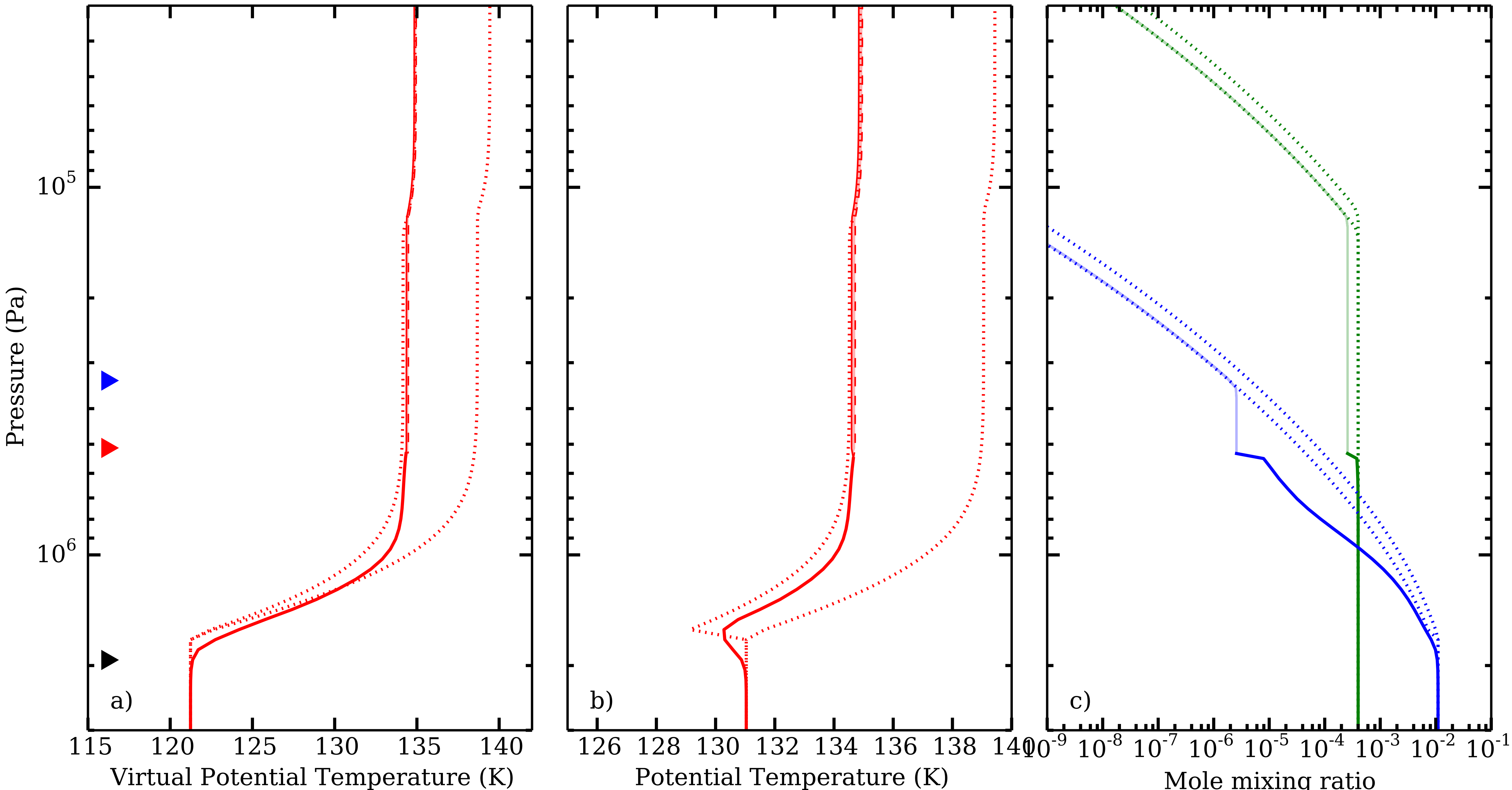

Step # 14: Year = 8.2

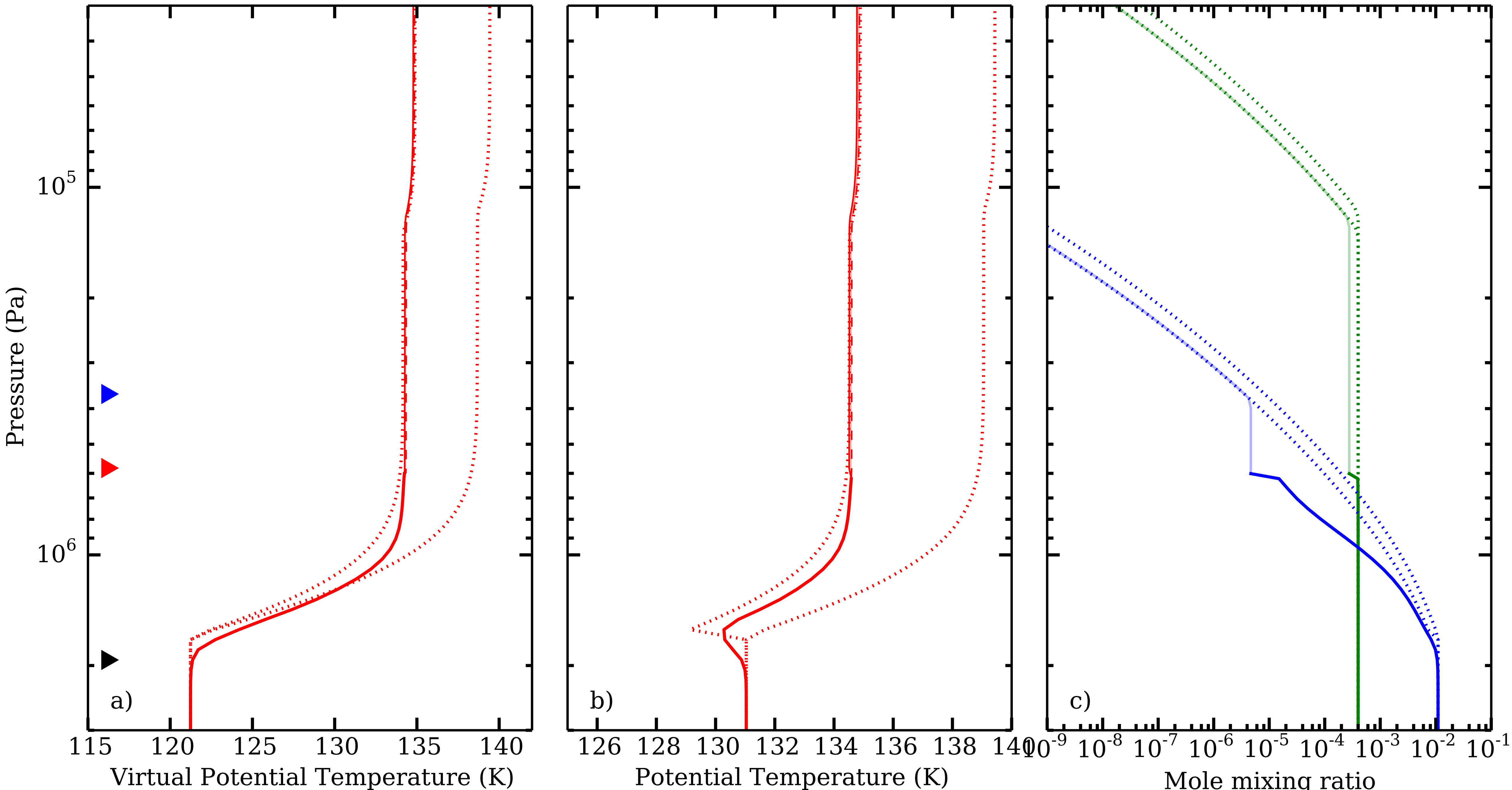

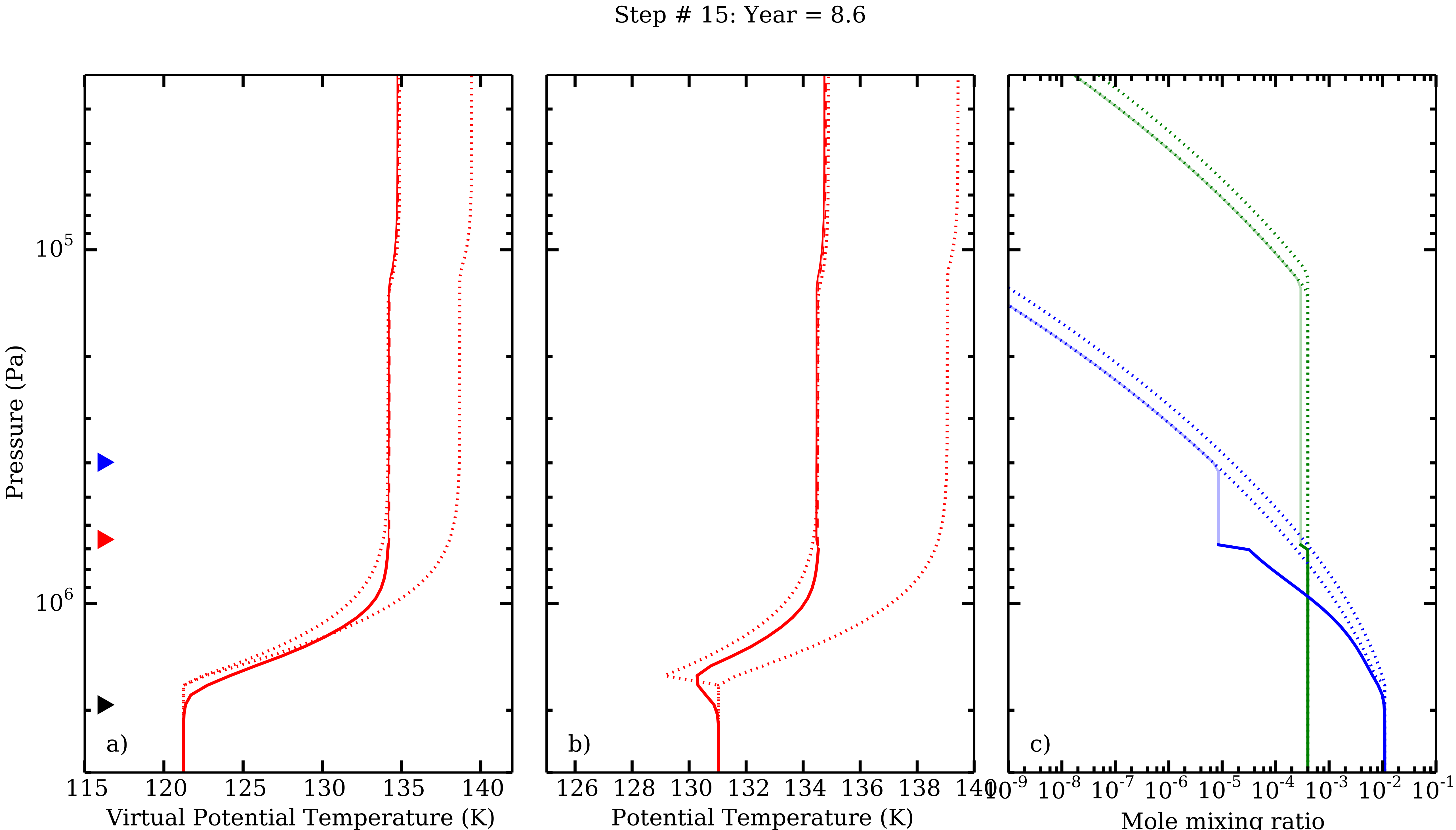
Step # 15: Year = 8.6
Pressure (Pa)
10^5
10^6
a)
115
120
125
130
135
140
Virtual Potential Temperature (K)
b)
126
128
130
132
134
136
138
140
Potential Temperature (K)
c)
10^{-9}
10^{-8}
10^{-7}
10^{-6}
10^{-5}
10^{-4}
10^{-3}
10^{-2}
10^{-1}
Mole mixing ratio

Step # 16: Year = 9.4

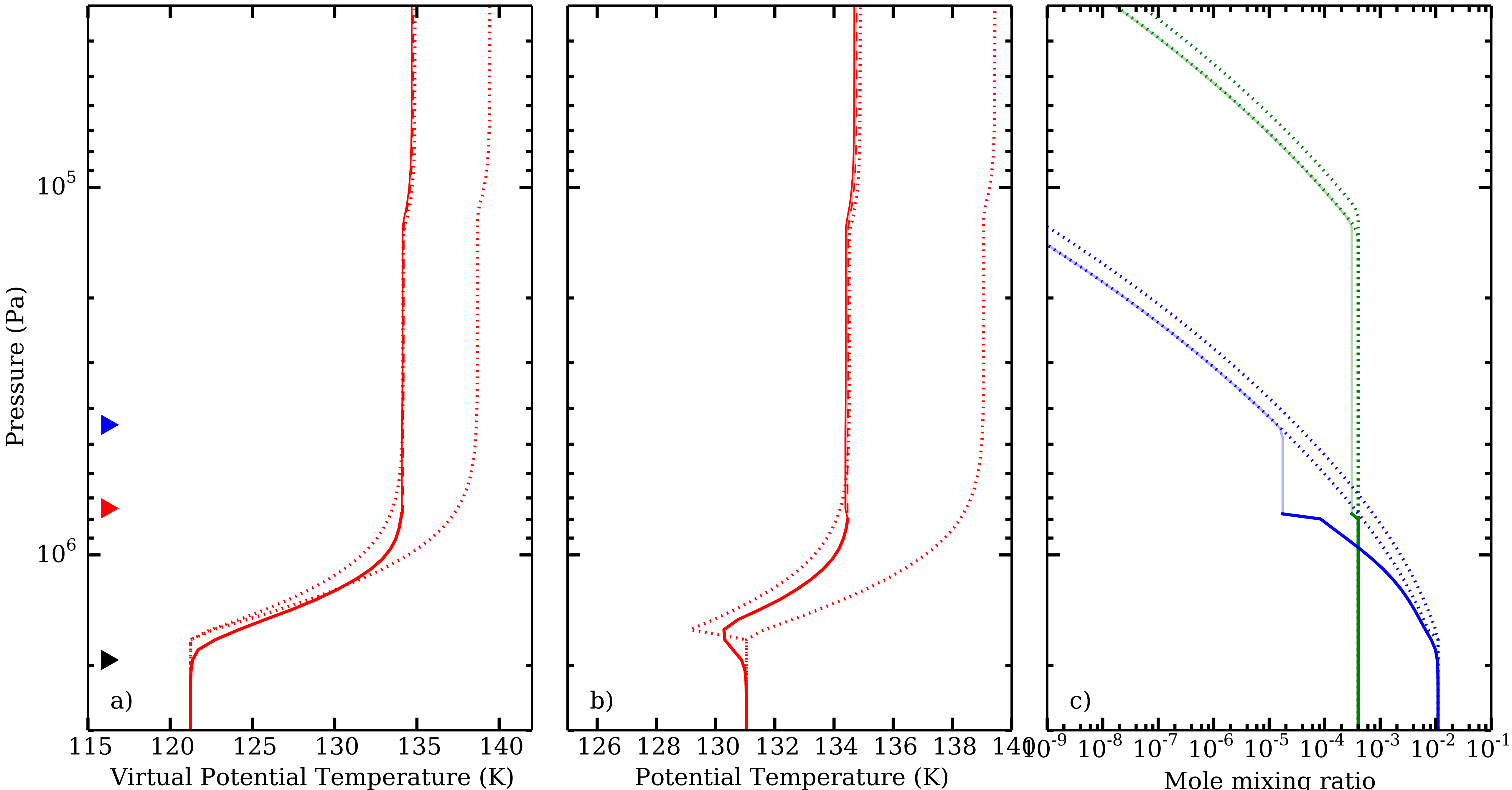

Step # 17: Year = 11.5

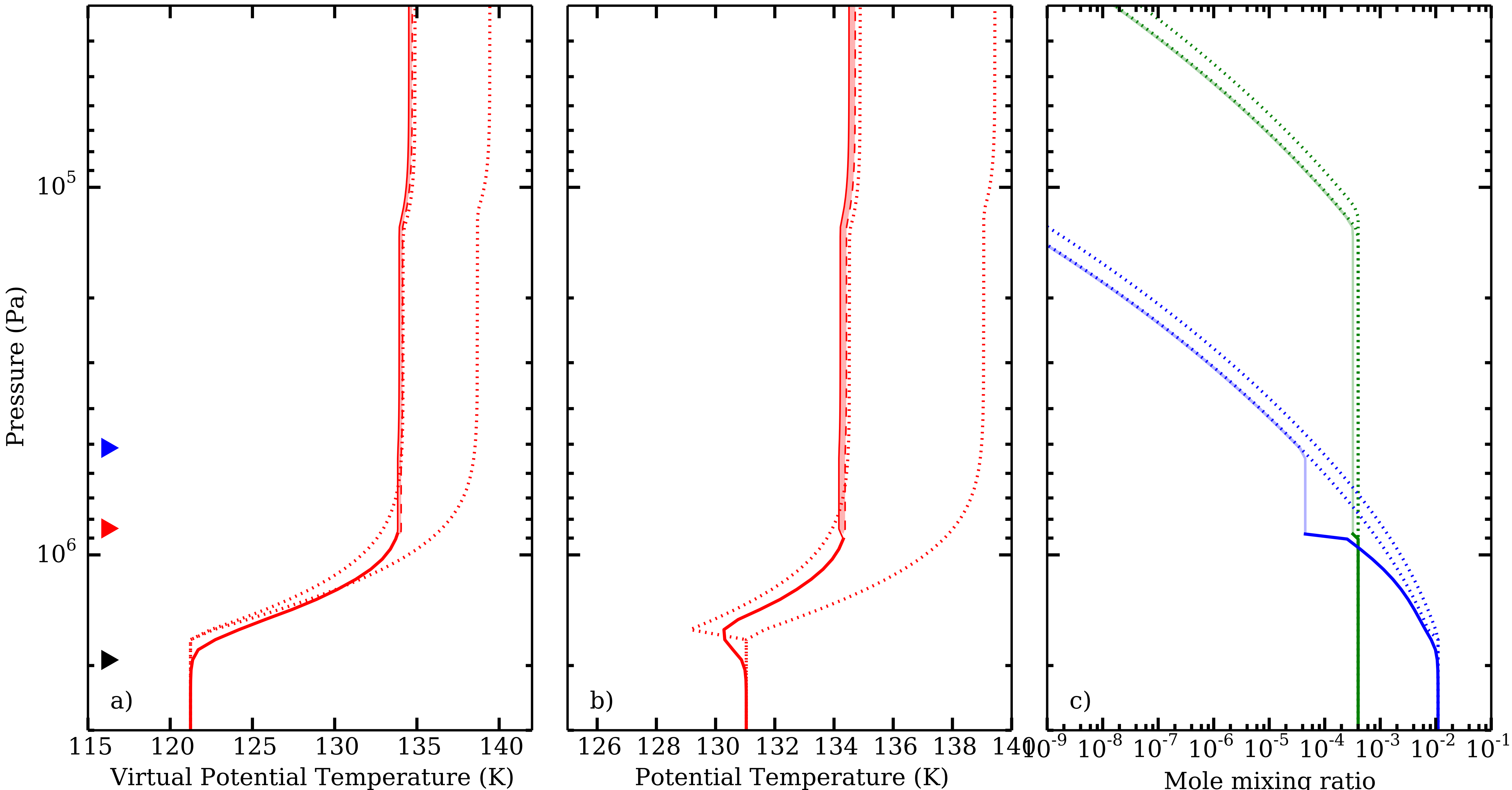

Step # 18: Year = 18.1

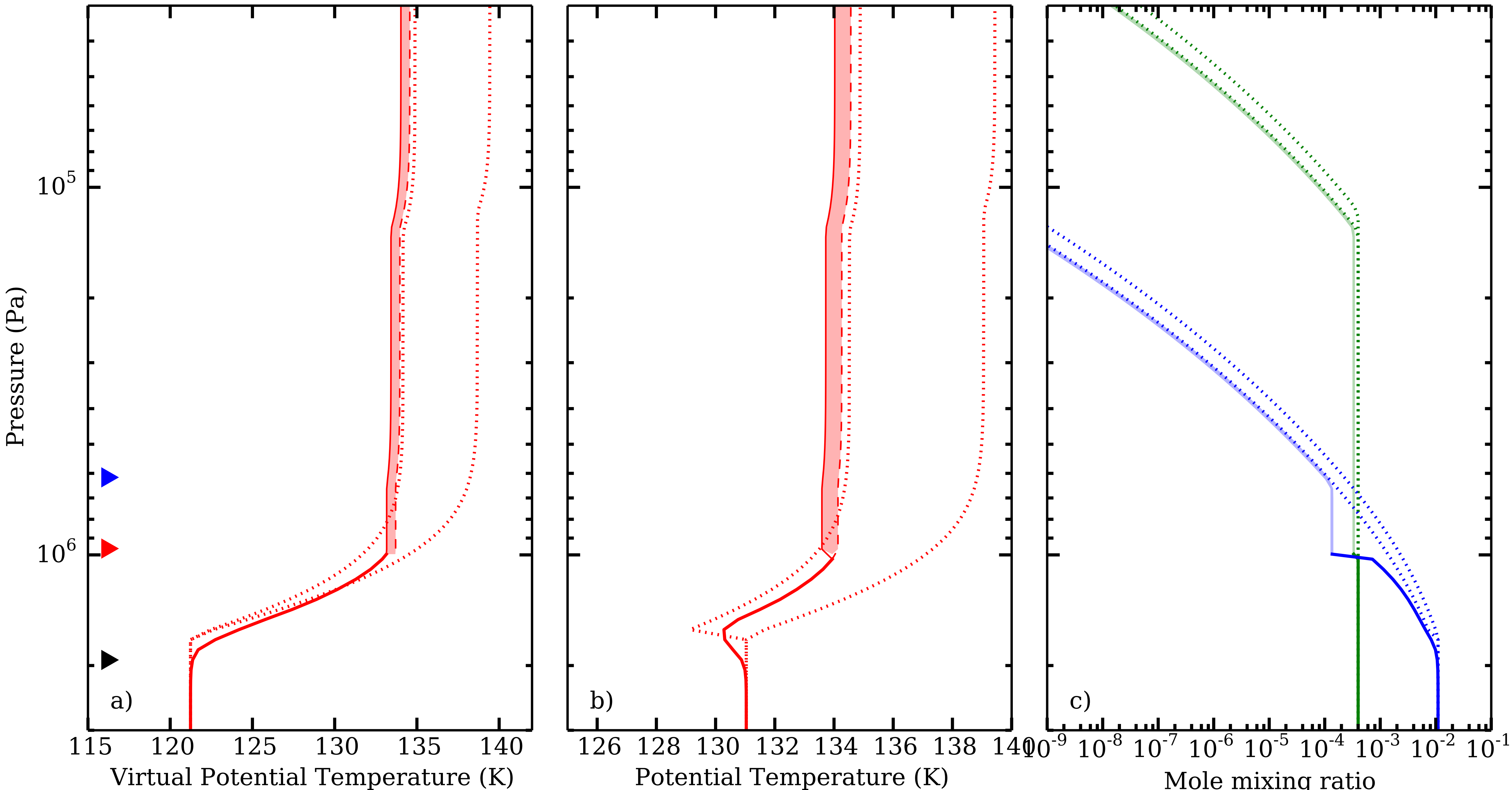

Step # 19: Year = 32.8

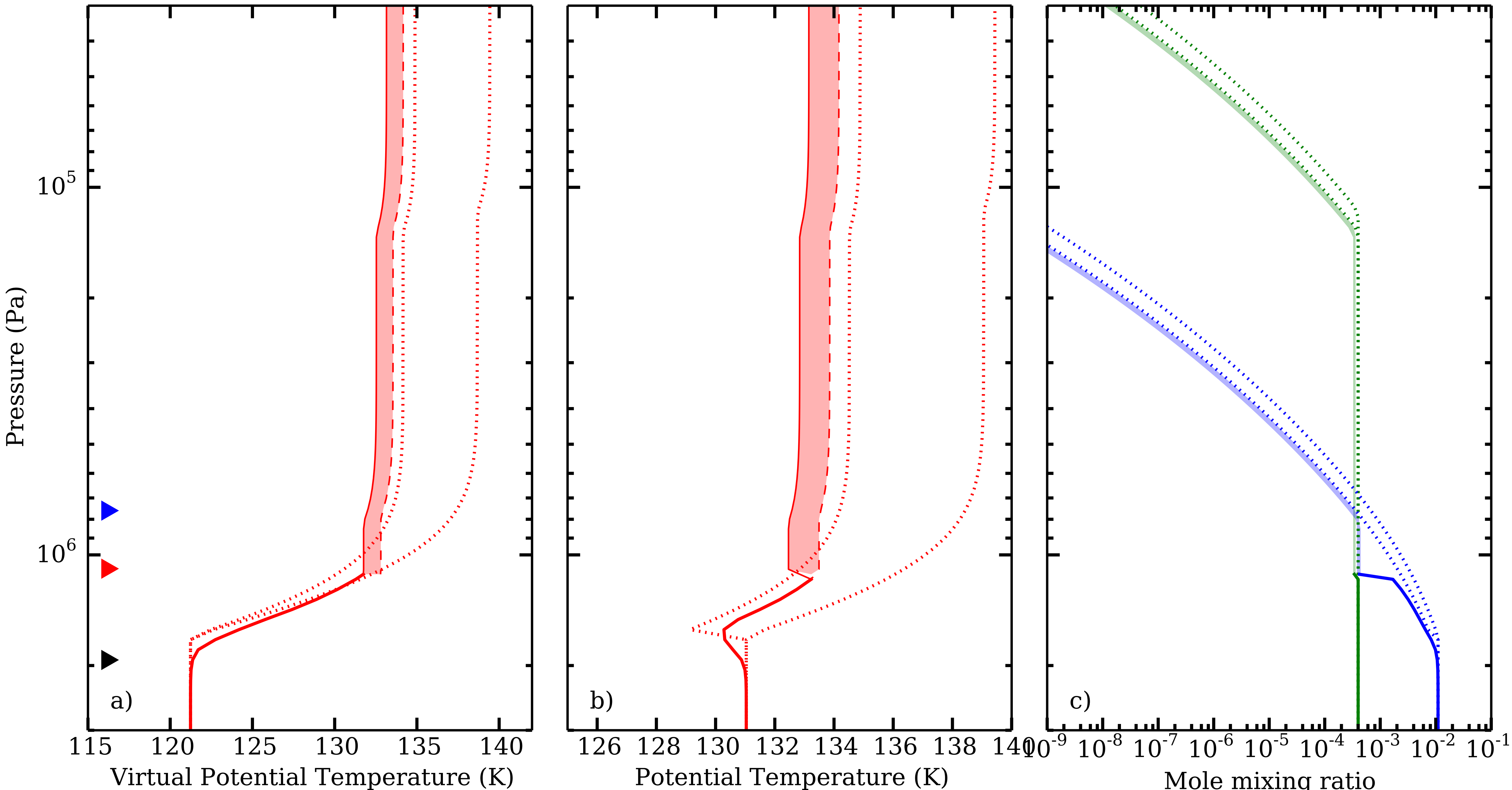

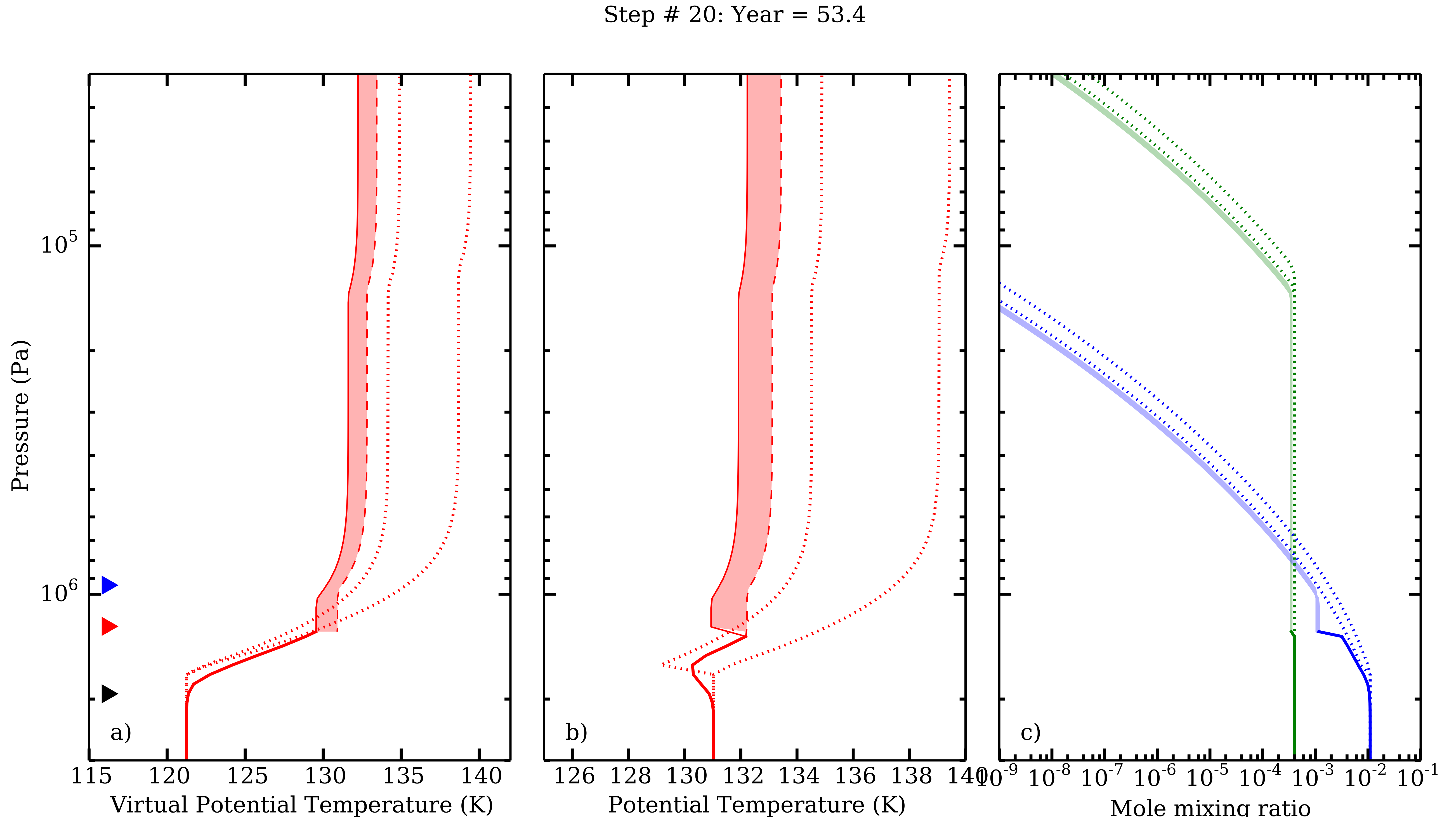
Step # 20: Year = 53.4
Pressure (Pa)
10^5
10^6
a)
115
120
125
130
135
140
Virtual Potential Temperature (K)
b)
126
128
130
132
134
136
138
140
Potential Temperature (K)
c)
10^{-9}
10^{-8}
10^{-7}
10^{-6}
10^{-5}
10^{-4}
10^{-3}
10^{-2}
10^{-1}
Mole mixing ratio

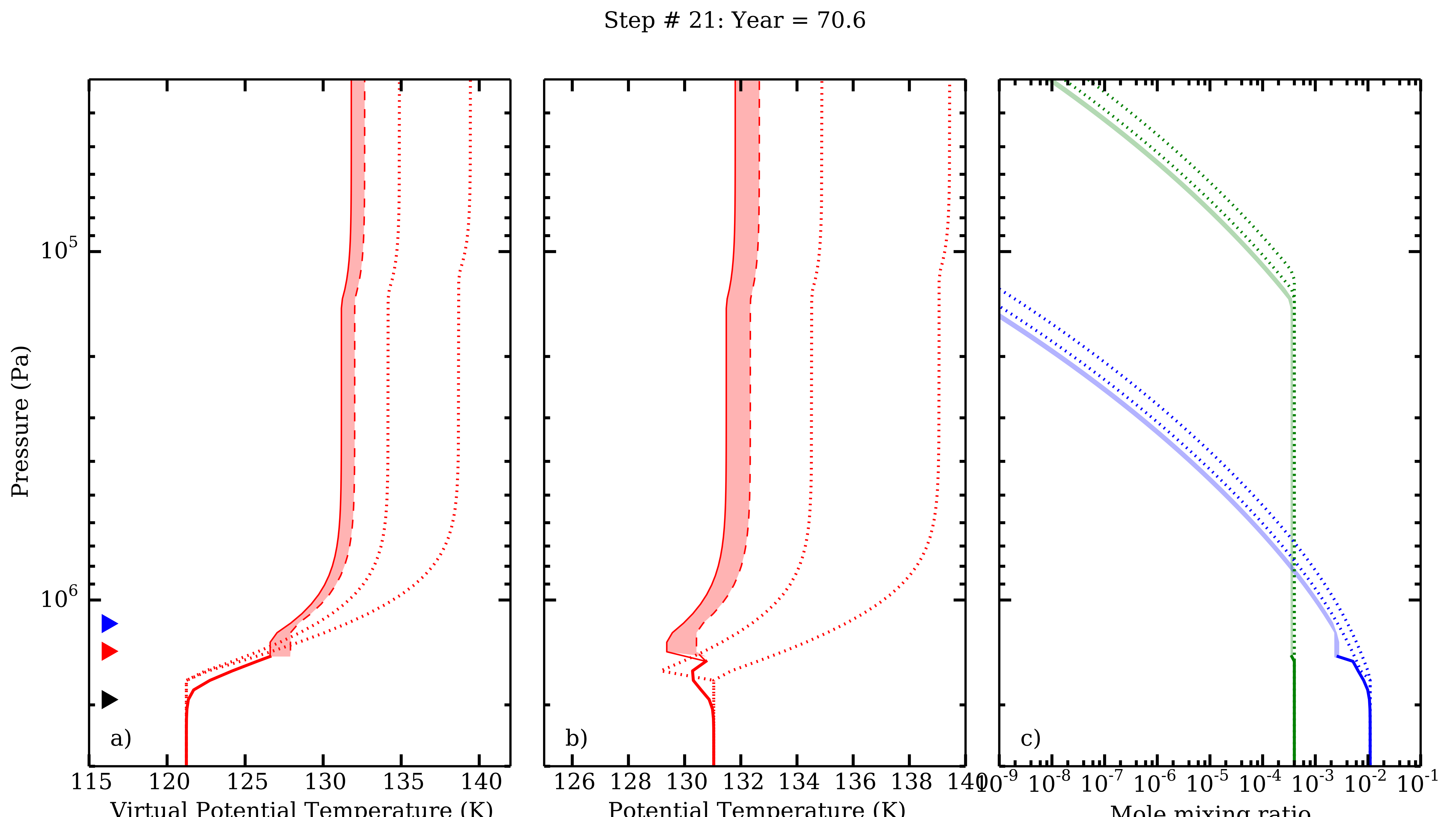

Step # 21: Year = 70.6
Pressure (Pa)
10^5
10^6
a)
b)
c)
115 120 125 130 135 140
Virtual Potential Temperature (K)
126 128 130 132 134 136 138 140
Potential Temperature (K)
10^{-9} 10^{-8} 10^{-7} 10^{-6} 10^{-5} 10^{-4} 10^{-3} 10^{-2} 10^{-1}
Mole mixing ratio

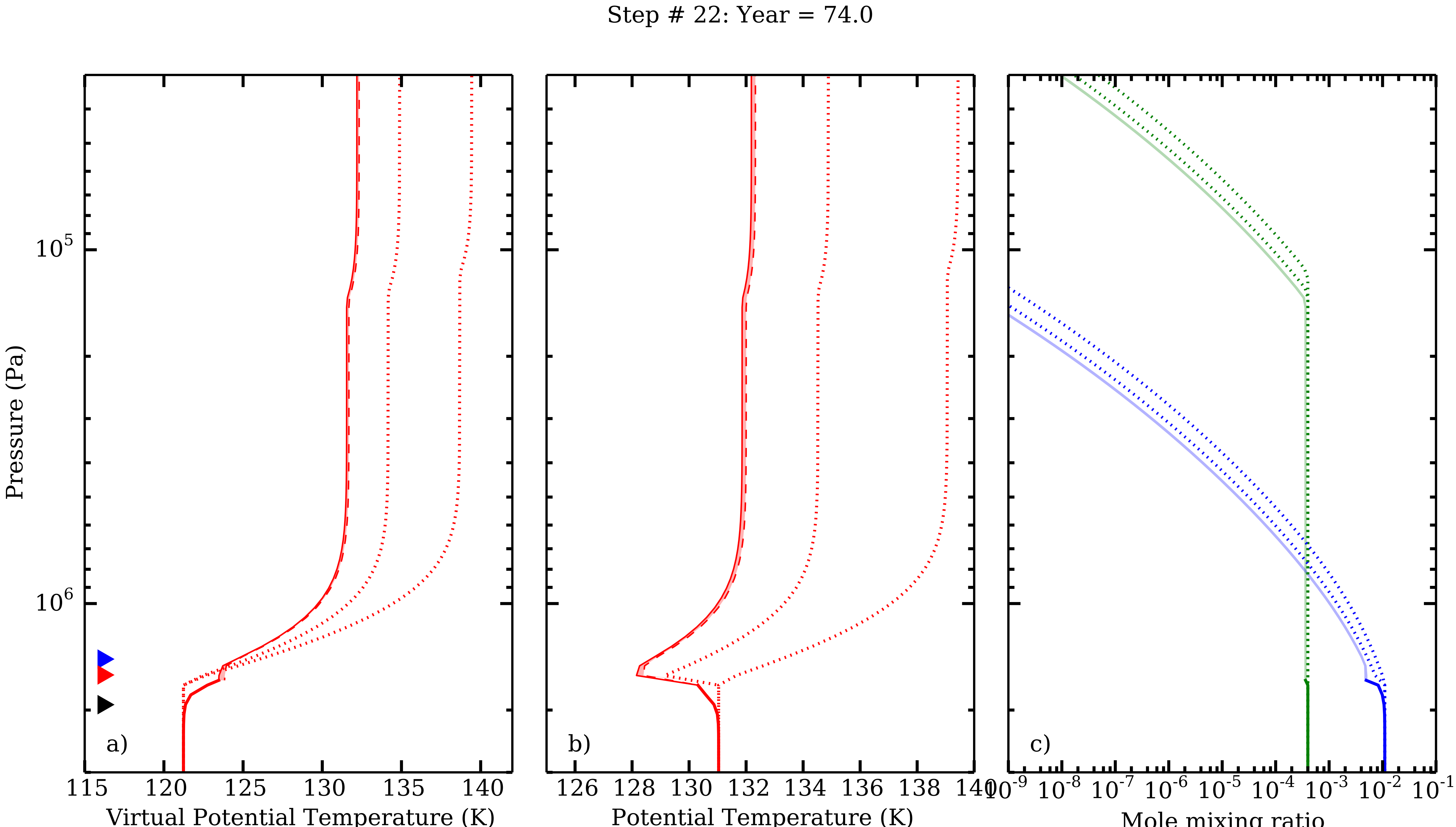
Step # 22: Year = 74.0
Pressure (Pa)
10^5
10^6
a)
b)
c)
115 120 125 130 135 140
Virtual Potential Temperature (K)
126 128 130 132 134 136 138 140
Potential Temperature (K)
10^-9 10^-8 10^-7 10^-6 10^-5 10^-4 10^-3 10^-2 10^-1
Mole mixing ratio